Final Report Submitted to the
National Aeronautics and Space Administration

February 29, 2004

Contract Number: NAS5-31370

Land Surface Temperature Measurements from EOS MODIS Data

MODIS Team Member
PRINCIPAL INVESTIGATOR

ZHENGMING WAN

P.I.'s Address:

Institute for Computational Earth System Science
University of California
Santa Barbara, CA 93106-3060

phone: (805)893-4541
Fax no: (805)893-2578
E-mail: wan@icess.ucsb.edu

Abstract

This report summarizes the accomplishments made by the MODIS LST (Land-Surface Temperature) group at University of California, Santa Barbara, under NASA Contract NAS5-31370 in the period from January 15, 1992 to February 29, 2004. Version 1 of the MODIS Land-Surface Temperature Algorithm Theoretical Basis Document (ATBD) was reviewed in June 1994, version 2 reviewed in November 1994, version 3.1 in August 1996, and version 3.3 updated in April 1999. Based on the ATBD, two LST algorithms were developed, one is the generalized split-window algorithm and another is the physics-based day/night LST algorithm. These two LST algorithms were implemented into the production generation executive code (PGE16) for the daily standard MODIS LST products at level-2 (MOD11_L2) and level-3 (MOD11A1 at 1km resolution and MOD11B1 at 5km resolution). PGE codes for 8-day 1km LST product (MOD11A2) and the daily, 8-day and monthly LST products at 0.05 degree latitude/longitude climate model grids (CMG) were also delivered. Four to six field campaigns were conducted each year since 2000 to validate the daily LST products generated by PGE16 and the calibration accuracies of the MODIS TIR bands used for the LST/emissivity retrieval from versions 2-4 of Terra MODIS data and versions 3-4 of Aqua MODIS data. Validation results from temperature-based and radiance-based methods indicate that the MODIS LST accuracy is better than 1° C in most clear-sky cases in the range from -10 to 58° C. One of the major lessons learnt from multi-year temporal analysis of the consistent V4 daily Terra MODIS LST products in 2000-2003 over some selected target areas including lakes, snow/ice fields, and semi-arid sites is that there are variable numbers of cloud-contaminated LSTs in the MODIS LST products depending on surface elevation, land cover types, and atmospheric conditions. A cloud-screen scheme with constraints on spatial and temporal variations in LSTs was developed to remove cloud-contaminated LSTs. The 5km LST product was indirectly validated through comparisons to the 1km LST product. Twenty three papers related to the LST research work were published in journals over the last decade.

1. Introduction

Before the launch of the first Moderate Resolution Imaging Spectroradiometer (MODIS) on the Earth Observing System (EOS) morning platform named Terra on 18 December 1999 (Guenther et al., 2002), the MODIS LST research was focused on the following pre-launch activities: (1) make atmospheric radiative transfer simulations of the MODIS thermal infrared (TIR) bands in various atmospheric and surface conditions based on the specifications of the MODIS; (2) analyze existing LST methods and develop prototype MODIS LST algorithms; (3) develop a TIR

instrumentation strategy and make custom refinements of TIR spectrometers to improve the accuracies of land-surface emissivity measurements in the laboratory and in the field, and land-surface temperature measurements in field campaigns; (4) validate the prototype MODIS LST algorithms with the MODIS Airborne Simulator (MAS) data; (5) write and update the MODIS LST ATBD; and (6) develop and deliver the MODIS LST PGE code (PGE16).

After the TIR bands in the Terra MODIS were stabilized in late February 2000, the beta version of the MODIS LST products was generated with the initial PGE16 code. This code has been refined in versions 2, 3 and 4 in the period from late 2000 to late 2002. Since June 2000, a series of field campaigns were conducted to validate the daily MODIS LST product in these versions. The V4 PGE16 code has been used since late December 2002 in the reprocessing for early MODIS data and the forward processing for new MODIS data. After the V4 reprocessing of Terra MODIS data was completed in December 2003, there are four years of consistent V4 Terra MODIS LST products. The second MODIS instrument was launched on the EOS afternoon platform named Aqua on 4 May 2002. Since February 2004, the V4 PGE16 code has been used in the reprocessing and forward processing of Aqua MODIS data.

This report will only highlight the major accomplishments and present the current status of the MODIS LST products and lessons learnt from the validation and analysis of V4 LST products. Details can be found in previous technical reports and published journal papers that will be listed at the end of this report.

2. Accomplishments

2.1 Theoretical Basis of MODIS LST Retrieval

Comprehensive atmospheric radiative transfer simulations were made for the MODIS TIR bands with an accurate atmospheric radiative transfer code developed by the P.I. based on the adding/doubling method (Wiscombe, 1976) and the "exponential-sum fitting" (Wiscombe and Evans, 1977) formulation of radiative transmission functions of the molecular absorption modeled in LOWTRAN7 (Kneizys et al, 1988) and MODTRAN3 (Berk et al, 1989) in the 90s. The scattering and absorption of the average aerosol distribution were also considered in the simulations (Wan and Li, 1997). Since 2000 the MODTRAN4 code (Berk et al, 1999) has been used in radiative transfer simulations.

In clear-sky conditions, the spectral infrared radiance $L(\lambda, \mu)$ at the top of the atmosphere is composed of surface thermal emittance, thermal path radiance $L_a(\lambda, \mu)$, path radiance resulting

from scattering of solar radiation $L_s(\lambda, \mu, \mu_o, \varphi_o)$, solar beam and downward solar diffuse radiation and atmospheric thermal radiation reflected by the surface, i.e.,

$$L(\lambda, \mu) = t_1(\lambda, \mu)\, \varepsilon(\lambda, \mu)\, B(\lambda, T_s) + L_a(\lambda, \mu) + L_s(\lambda, \mu, \mu_o, \varphi_o)$$
$$+ t_2(\lambda, \mu, \mu_o)\, \mu_o\, E_o(\lambda)\, f_r(\mu; \mu_o, \varphi_o)$$
$$+ \int\int \mu'\, f_r(\mu; \mu', \varphi')\, [\, t_3(\lambda, \mu)\, L_d(\lambda, -\mu', \varphi') + t_4(\lambda, \mu)\, L_t(\lambda, -\mu', \varphi')\,]\, d\mu'\, d\varphi' \qquad (1)$$

where μ is cosine of the viewing zenith angle, $\varepsilon(\lambda, \mu)$ is the surface spectral emissivity, $B(\lambda, T_s)$ is the radiance emitted by a blackbody at surface temperature T_s , $E_o(\lambda)$ is the spectral solar irradiance incident on the top of the atmosphere (normal to the beam), μ_o is cosine of the solar zenith angle, φ_o is the relative azimuth between the viewing direction and the solar beam direction, $f_r(\mu; \mu_o, \varphi_o)$ is the bidirectional reflectance distribution function (BRDF) for the solar beam, $L_d(\lambda, -\mu', \varphi')$ is the downward solar diffuse radiance, $L_t(\lambda, -\mu', \varphi')$ is the atmospheric downward thermal radiance, their incident direction is represented by $-\mu'$and φ', $f_r(\mu; \mu', \varphi')$ is the BRDF for $L_d(\lambda, -\mu', \varphi')$ and $L_t(\lambda, -\mu', \varphi')$, and t_i , i = 1- 4 are transmission functions for the corresponding terms. Eq. (1) is the theoretical basis for the thermal infrared remote sensing. The wavelength, λ, in (1) is the wavelength center of a very narrow wavelength interval because there is no way to measure the exact monochromatic signal as a continuous function of wavelength by most TIR sensors. In a narrow wavelength interval, all t_i functions may be assumed equal.

For thermal infrared bands with moderate bandwidths such as in MODIS and AVHRR, all the terms in (1) must be integrated over the whole bandwidths with the spectral response function of each band as weights. The measured spectral response functions of the MODIS TIR bands were used to define the band-averaged terms in (1). We avoided the use of effective wavelength in calculations of band-averaged radiance, emissivity, and other terms because of uncertainties in the effective wavelength due to temperature changes and different within-band spectral variations in each terms. When we deal with the band-averaged terms for MODIS TIR bands, all the within-band spectral features such as in surface emissivities are unknown in general. Therefore, we have to separate the emissivity and BRDF or reflectance terms from the radiance or radiation terms in the integral of (1) and represent them in corresponding band-averaged emissivity or reflectance values. Errors would be inevitably introduced in this de-convolution process.

The maximum errors may be up to a few percents if there are strong spectral variations for some surface materials in MODIS TIR bands. This is one of the main reasons for the accuracy specification of 1K for the MODIS LST product, in contrast to the accuracy specification of 0.3K for the MODIS sea-surface temperature (SST) product.

2.2 Development of Generalized Split-window LST Algorithm

We evaluated various split-window LST algorithms (Price, 1984; Becker, 1987; Wan and Dozier, 1989; Becker and Li, 1990b; Sobrino et al., 1991; Vidal 1991; Kerr et al., 1992; Ottle and Stoll, 1993; Prata, 1994) in their abilities to deal with the difficulties in the LST retrieval (Wan and Dozier, 1989), i.e., considerable variation in surface emissivity for different land-surface materials (Salisbury and D'Aria, 1992a,b; Nerry et al., 1990) and the angular effects in the emissivity (Dozier and Warren, 1982; Labed and Stoll, 1991; Rees and James, 1992), wide ranges of the LST and atmospheric conditions, and the mixed-pixel problem. A generalized split-window algorithm was developed (Wan and Dozier, 1996) to retrieve LSTs from MODIS data for clear-sky pixels, in form of

$$T_s = C + [A_1 + A_2 (1 - \varepsilon) / \varepsilon + A_3 \Delta\varepsilon / \varepsilon^2] (T_{31} + T_{32}) / 2$$
$$+ [B_1 + B_2 (1 - \varepsilon) / \varepsilon + B_3 \Delta\varepsilon / \varepsilon^2] (T_{31} - T_{32}) / 2 \qquad (2)$$

where T_{31} and T_{32} are the brightness temperatures in bands 31 and 32, ε and $\Delta\varepsilon$ are the mean and difference of emissivities in these two bands. The retrieved T_s value is used as the LST science data set (SDS) value in the daily level-2 LST product (MOD11_L2).

The coefficients (A_i, B_i, and C) used in this LST algorithm were given by interpolation on a set of multi-dimensional look-up tables (LUT). The LUTs were obtained by linear regression of the MODIS simulation data from radiative transfer calculations over wide ranges of surface and atmospheric conditions. Improvements for the generalized split-window LST algorithm incorporated in the establishment of the LUTs include: 1) view-angle dependence, 2) column water vapor dependence, and 3) dependence on the atmospheric lower boundary temperature. The view-angle dependence is kept in one dimension of LUTs for a set of viewing angles covering the whole MODIS swath. This allows LST to be retrieved at higher accuracies for pixels at both small and large viewing zenith angles, with reduced sensitivities to the uncertainties in band emissivities. The column water vapor dependence is kept in another dimension of LUTs for a set of overlapping intervals of column water vapor, thus the information of water vapor provided in the MODIS atmospheric product is used as the most likely range of the water vapor rather than its

exact value because the uncertainties in the atmospheric water vapor may be large. Similarly, the information of the atmospheric lower boundary temperature provided in the MODIS atmospheric product is also used to improve the LST retrieval accuracy.

A TIR BRDF and emissivity model was developed (Snyder and Wan, 1998) to calculate the emissivities in MODIS bands 31 and 32 for land cover types (Snyder et al., 1998). It was shown that errors and uncertainties in the classification-based emissivities may be large in some cases such as in semi-arid and arid regions because of the large temporal and spatial variations in surface emissivities and lack of knowledge on the proper values of the measurement correction and volumetric factor in the BRDF/emissivity modeling, and the emissivity variation with viewing angle.

The daily MOD11A1 LST product is constructed with the results in the MOD11_L2 products of a day through mapping the SDSs of all pixels in MOD11_L2 products onto grids in the integerized sinusoidal (in V1-V3) or sinusoidal (in V4) projection and averaging the values in each 1km grid. The actual size of the 1km grid is 0.93km, which is approximately the nominal pixel size at the center of the MODIS swath (viewing at nadir) for the 1km TIR bands. As the scan angle increases from nadir, the pixel dimension grows until reaching about 2km along track and larger than 4km across track at either end of the scan (Masuoka et al., 1998). Therefore, the 1km MOD11A1 product may show spatial features in LSTs at the 1km scale only in variable portions where MODIS observes the surface at small viewing zenith angles.

2.3 Development of Physics-based Day/Night LST Algorithm

Li et al.(1999) evaluated the performance of six methods for extracting relative emissivity spectra from TIR data, including the two-channel temperature-independent spectral indices (TISI) method (Becker and Li, 1990a; Li and Becker, 1993) that is the basis for the method used to estimate surface reflectance and emissivity in the middle infrared bands with MODIS data (Petitcolin and Vermote, 2002); the reference channel method (Kahle et al., 1980); emissivity normalization method (Realmuto, 1990) that is used in the temperature and emissivity separation algorithm for Advanced Spaceborne Thermal Emission and Reflection Radiometer (ASTER) data (Gillespie et al., 1998); emissivity renormalization method that is a revised two-channel TISI method; the spectral ratio method (Watson, 1992); and alpha emissivity method (Kealy and Gabell, 1990). That paper shows that all the six methods are very sensitive to the atmospheric

correction errors particularly when the atmospheric effects are overcorrected. At the EOS AM1 Land Workshop in May 1996, John Price of the Peer Review Panel recommended that the coupling between land and atmosphere be handled properly in the algorithms for MODIS atmospheric and land products. Results of the collaboration between the UCSB MODIS LST group and the MODIS Atmosphere group at the University of Wisconsin at Madison show that atmospheric profiles and land-surface temperature/emissivity can be simultaneously retrieved better from day and night MODIS observations (Ma et al., 2000; Ma et al., 2002). However, this algorithm is too computationally time consuming to be used in operational code at this moment or in the near future. Therefore, a physics-based day/night LST algorithm (Wan and Li, 1997) was developed for the operational generation of the daily MODIS land-surface temperature/emissivity product from a pair of daytime and nighttime MODIS data in seven TIR bands (bands 20, 22-23, 29 and 31-33). This algorithm is based on a set of equations of radiance in MODIS band j

$$L(j) = t_1(j)\,\varepsilon(j)\,B_j(Ts) + L_a(j) + L_s(j) + [t_2(j)\,\alpha\,\mu_o\,E_o(j) + t_3(j)\,E_d(j) + t_4(j)\,E_t(j)]\,[1-\varepsilon(j)]\,/\,\pi \qquad (3)$$

where all the terms are band-averaged ones of the corresponding terms in Eq. (1), and α is anisotropic factor defined as $\pi\, f_r(\mu;\, \mu_o,\, \varphi_o)\,/\,r$ for the solar beam term, r is reflectance of the surface like Lambertian surface for band-averaged solar diffuse irradiance $E_d(j)$ and atmospheric downward thermal irradiance $E_t(j)$, $r = 1 - \varepsilon$ according to Kirchhoff's law. The solar radiation terms make significant contributions in (3) during day for bands 20, 22 and 23 in the 3.5-4.2μm spectral range, but they are negligible for bands 29 and 31-33 in the 8-13.5μm spectral range.

Using a pair of daytime and nighttime MODIS data in seven bands provides 14 observations. So in the day/night algorithm, there may be maximum of 14 unknown variables. In theory, the minimal set of the surface variables includes 7 band emissivities, and daytime and nighttime surface temperatures. There are five unknowns left for other variables. Because of the close coupling between land surface and atmosphere, uncertainties in surface reflectance/emissivity may result in large errors in the atmospheric temperature/water vapor retrieval (Plokhenko and Menzel, 2000). These errors could exist in the shape of the retrieved temperature/humidity profile, and in the values of atmospheric temperature at the surface level (T_a) and column water vapor (cwv). Atmospheric radiative transfer simulations show that the MODIS radiances in the above seven TIR bands are relatively less sensitive to changes in the shapes of temperature and water vapor profiles. Therefore, we set four atmospheric variables (T_a and cwv, for daytime and nighttime, respectively). The last unknown is used for the anisotropic factor of the solar beam BRDF at the surface. This day/night algorithm is the first operational LST algorithm capable of adjusting the uncertainties in atmospheric temperature and column water vapor for a better

retrieval of the surface emissivity and temperature without a complicated simultaneous retrieval of surface variables and atmospheric profiles.

The daytime and nighttime MODIS radiance values are co-registered on grids in sinusoidal projection. The selection of the grid size mainly depends on the pixel size of MODIS TIR bands because the accuracy of the MODIS pixel geo-location is much better than the specification of 150m (Wolfe et al., 2002). A 5km grid size (actually 4.63km x 4.63km) was selected because the MODIS TIR pixel is larger than 4km x 2km by the MODIS swath edges.

2.4 Development of PGE Code for MODIS LST Products

The generalized split-window LST algorithm and the day/night LST algorithm were implemented into the production generation executive (PGE) code for the daily standard MODIS LST products at level 2 (MOD11_L2) and level 3 (MOD11A1 and MOD11B1). This PGE code was revised and improved not only for providing better quality of the LST products but also for its computational efficiency through careful designs of LUTs and data structures, and parallel processing capabilities.

The quality of V4 MODIS LST products has improved due to higher-quality MODIS products used as inputs, and the following refinements made to the version-4 MODIS LST PGE code: (1) update of the LUTs used in the day/night LST algorithm; (2) processing lake pixels in clear-sky at a confidence of 66% or higher; (3) using BRDF Albedo Parameters of the MODIS 16-day BRDF product (MOD43B1C) as an optional input; (4) separating the range of viewing zenith angles into five sub-ranges (0-24 °, 24-38 °, 38-49 °, 49-58 °, and 58-65 °) instead of four as we did in the V3 code; and (5) incorporating a split-window method into the day/night algorithm to ensure that the retrieved emissivities can be used by split-window algorithms.

2.5 The Development of TIR Instrumentation

Recognizing the necessity of validating the accuracies of MODIS TIR data and MODIS LST product, the UCSB MODIS LST team has pursued a TIR instrumentation strategy since early 90s through gradual purchasing and improvements of TIR instruments. A series of calibration procedures were developed to assure the accurate measurements of land-surface emissivity and temperature in the laboratory and field in order to validate the LST algorithm and product (Snyder et al., 1997a; Snyder et al., 1997b). A spectral infrared bidirectional reflectance and

emissivity (SIBRE) system, which includes a hemispherical pointing system, FTIR spectrometer, a TIR source, and reference plates, was developed for measurements of TIR BRDF and emissivity (Snyder and Wan, 1996). A FTIR spectrometer-integrating sphere system was developed to measure reflectance/emissivity spectra of terrestrial material samples. Measured spectral data were posted in the MODIS UCSB Emissivity Library (http://www.icess.ucsb.edu/modis/EMIS/html/em.html). The emissivity spectra in this library have been used by the MODIS Atmosphere group as the training data set for the improvement of the MODIS atmospheric profile algorithm. Samples of the atmospheric profile product from Aqua MODIS over northern Sahara show improvements due to the use of these emissivity spectra (Seemann, personal communication). A ball-based floating system, shown in the left side of Fig. 1, for a TIR radiometer to measure lake surface temperatures was designed to keep small cross sections in the water and air so that its disturbance on the water surface and effect on the radiometric measurement are negligible (Wan et al., 2002a). The instrumentation also includes radiosonding systems for measurements of atmospheric temperature and water vapor profiles, a Bomem TIR spectroradiometer (MR100), shown in the right side of Fig. 1, for measurements of sky radiance and TIR radiation from the surface in the field, and blackbody systems for calibration of TIR radiometers.

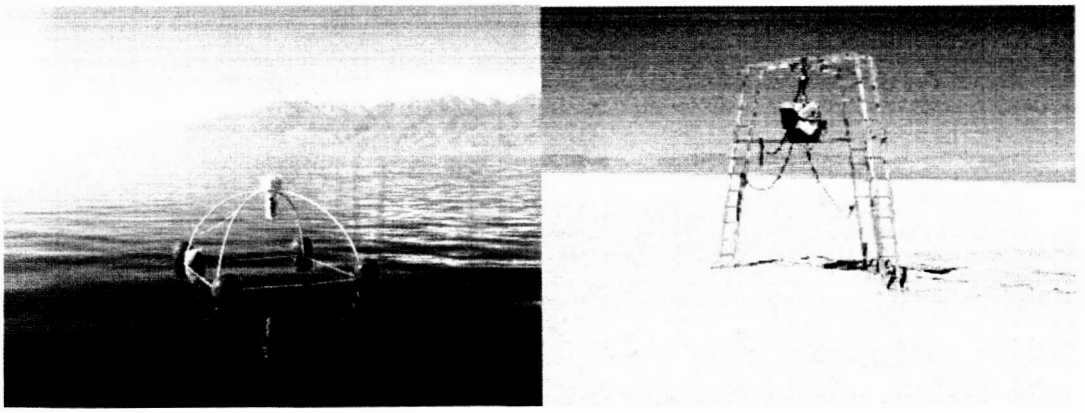

Fig. 1, A ball-based floating system of TIR radiometer deployed in Walker Lake, NV (left), and the Bomem TIR spectroradiometer (MR100) deployed in Railroad Valley, NV (right).

2.5.1, Conventional temperature-based method for LST validation

Multiple TIR radiometers are used to measure the surface radiometric temperature. The effects of surface emissivity and reflected atmospheric radiation are corrected to obtain the in-situ measured

LST using the emissivity value based on land-cover, sample measurements and atmospheric radiative transfer simulations. Comparisons between the in-situ LSTs and MODIS LSTs give the accuracy of MODIS LSTs. This method was used in most field campaigns for validating the MODIS TIR calibration and MODIS LST products (Wan et al., 2002a, 2002b, 2004b).

2.5.2, Advanced radiance-based method for LST validation

Radiosonde balloons are launched to measure the atmospheric temperature and water vapor profiles around the MODIS overpass time. Based on the measured atmospheric profile, MODIS LST and the spectral emissivity value measured in the field or estimated from land-cover and/or sample measurements, atmospheric radiative transfer simulations are made to calculate the brightness temperature T_b in MODIS band 31. The difference between the calculated T_b and MODIS T_b values divided by the atmospheric transmission in band 31 can be used to estimate the accuracy of the MODIS LST. The main advantage of this method is that it works for both daytime and nighttime. This method requires accurate atmospheric temperature and water vapor profiles, such as in Fig. 2 measured in the June 2003 Railroad Valley field campaign, and accurate atmospheric radiative transfer code. The excellent agreements, as shown in Fig. 3, between the measured spectral sky radiance and the radiance calculated with MODTRAN4.0 (Berk et al., 1999) based on measured atmospheric profiles provide a solid evidence of the good quality of the Bomem TIR spectroradiometer and the radiative transfer code MODTRAN4.

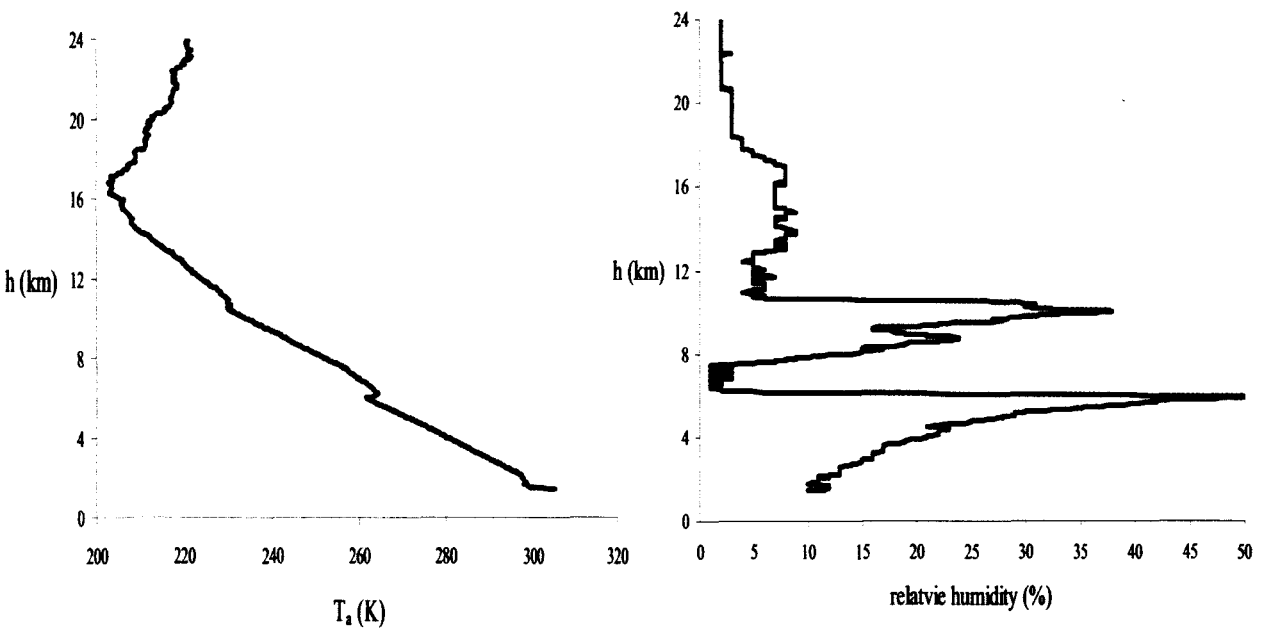

Fig. 2, Atmospheric temperature (left) and water vapor (right) profiles measured in Railroad Valley, NV in the period from 10:30am to 12:30pm, 29 June 2003.

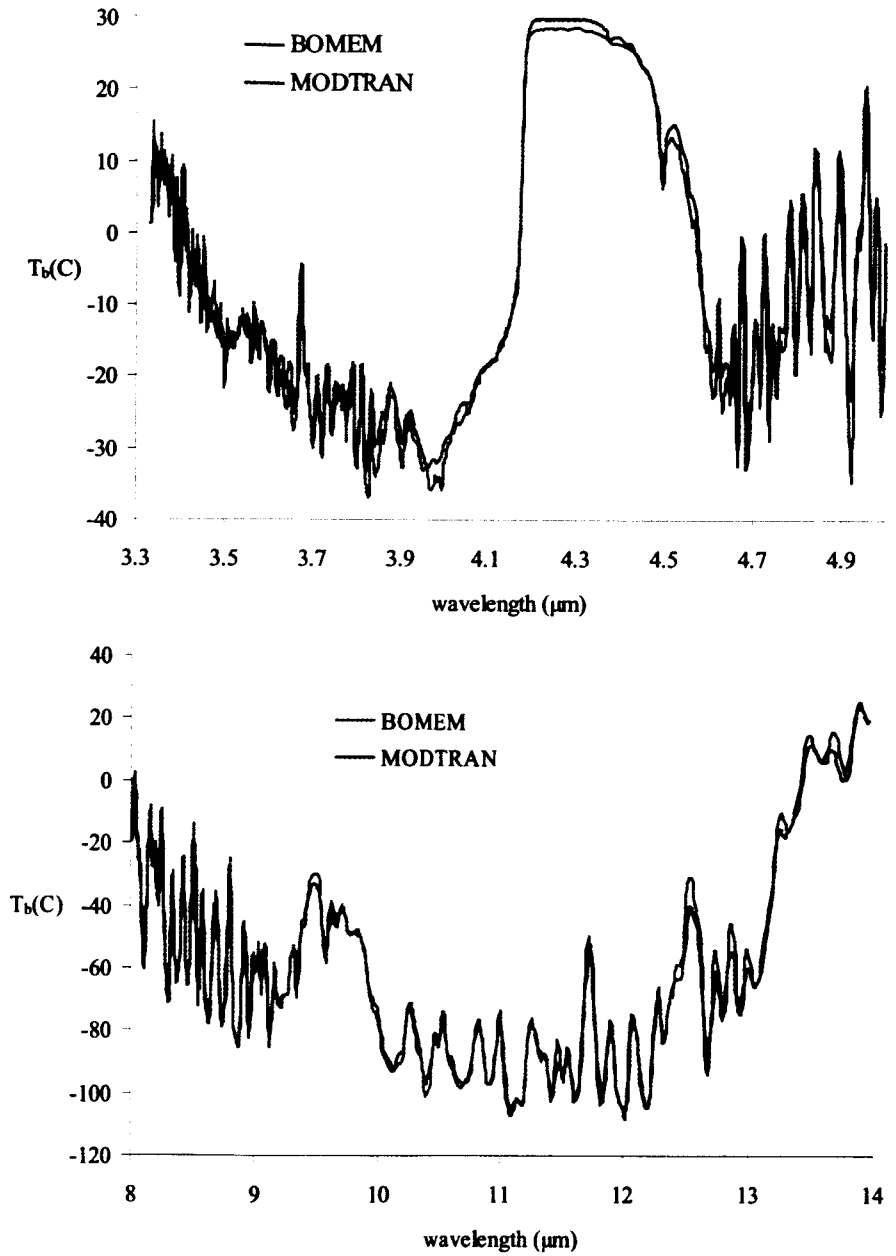

Fig. 3, Comparison of sky radiances measured by Bomem at 10:30am and calculated by MODTRAN4 based on atmospheric profiles measured during 10:30am and 12:30pm in Railroad Valley, NV, on 6/29/2003. The large discrepancies around 4μm and 4.2-4.4μm may attribute at least in part to the temporal changes in atmospheric temperature during the two hours.

In the June 2003 Railroad Valley field campaign, besides the four TIR radiometers deployed in the central portion of the Railroad Valley playa, the Bomem TIR spectroradiometer (MR100) was also deployed at 38.4817°N 115.6905°W, by the center of the rectangular consisting of the

four TIR radiometers. The size of the rectangular is about 500m by 500m. Six sounding balloons that carry Vaisala radiosonde RS90-A were launched in clear-sky days to measure the atmospheric temperature and water vapor profiles.

We measured the surface-leaving radiance under sunshine and shadow conditions with the MR100 spectroradiometer. A simplified version of the day/night method (Wan and Li, 1997) was used to retrieve surface temperatures under sunshine and shadow conditions, and emissivity values in seven bands. Once the playa surface temperature is determined, the measured spectral data were used to calculate the spectral emissivity of the playa surface, as shown in Fig. 4.

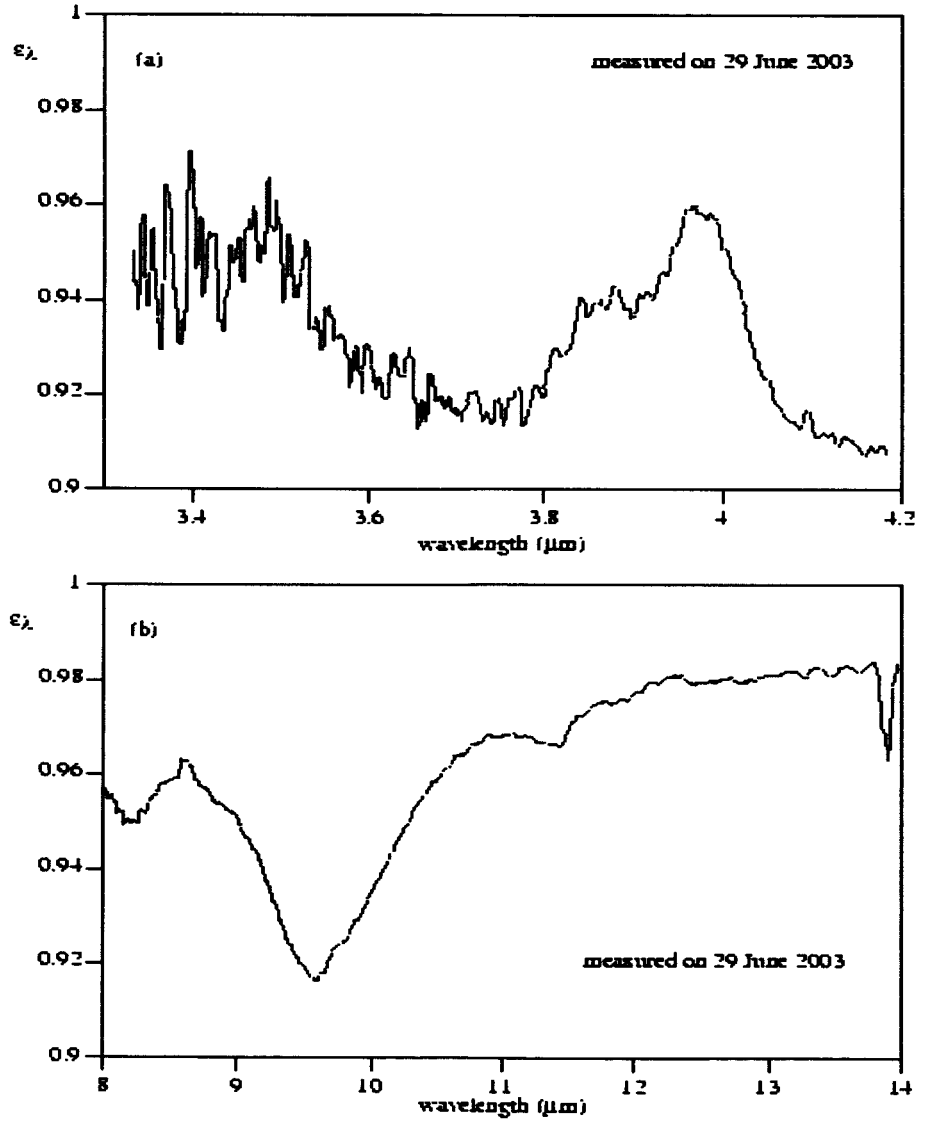

Fig. 4, Spectral emissivity of the playa surface measured with the sun/shadow method in Railroad Valley, NV, on 29 June 2003.

2.6 Validation of the MODIS TIR Data and LST Products

The UCSB MODIS team evaluated the channel-dependent noise and systematic error in MODIS TIR channel data with early MODIS data over lake and ocean sites in clear-sky days (Wan, 2002), and conducted a series of field campaigns beginning 2000 with in-situ measurements in various test sites including Lake Titicaca in Bolivia, Mono Lake, Bridgeport grassland and snow field, a rice field in California, Walker Lake and Railroad Valley silt playas in Nevada, and agricultural fields in Mississippi. The calibration accuracies of MODIS Airborne Simulator (MAS) TIR bands (Wan et al., 1999) and the MODIS TIR bands (Wan et al., 2002a), shown in Fig. 5, were evaluated with in-situ measurements in high altitude lakes.

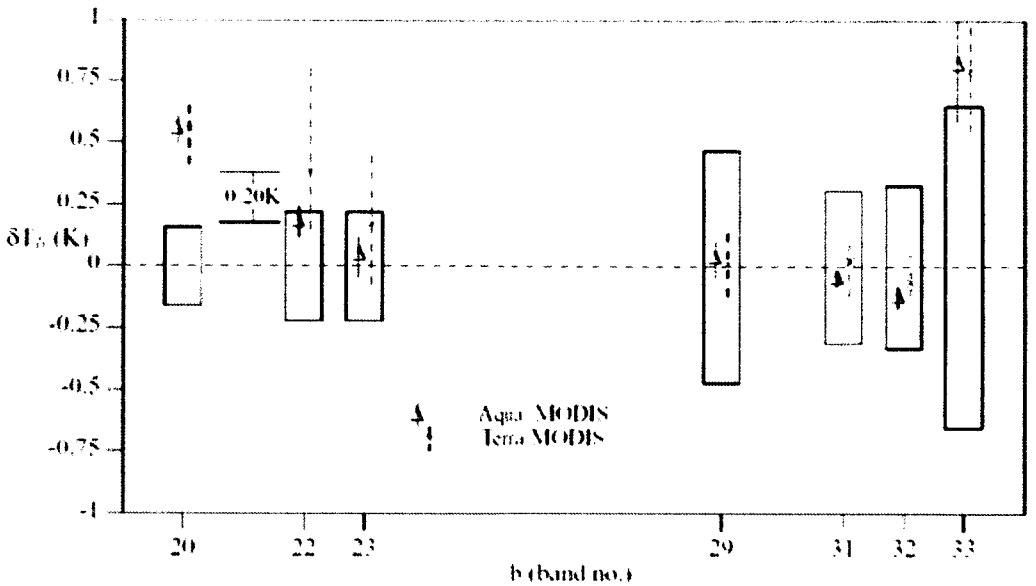

Fig. 5, Calibration bias in the Terra and Aqua MODIS TIR bands 20, 22, 23, 29, and 31-33 estimated from Walker Lake field campaigns in 2001 and 2003.

Four to six field campaigns were conducted each year in 2000-2003 to validate the daily LST products generated by PGE16. Validation results from temperature-based and radiance-based methods indicate the accuracy of daily MODIS LST product is better than 1 °C in most clear-sky cases in the range from -10 to 58 °C and the atmospheric column water vapor range of 0.4-4cm (Wan et al., 2002b; 2004b).

3. Current Status of the MODIS LST Products

The current (V4) MODIS LST products generated from Terra MODIS data are listed in Table I. Since starting the V4 reprocessing for Terra MODIS data in December 2002, the production rate

at the MODIS Data Processing System (MODAPS) is over 4X (processing more than 4 days of data each day) in the V4 reprocessing, plus 1X for the Terra forward processing and 1X for the Aqua forward processing. V4 Aqua MODIS LST products were released in early 2004. Quality assessments were performed with the MODIS LST science computing facility (SCF) at UCSB.

Table I, V4 Land-Surface Temperature (LST) products generated from Terra MODIS data. Visit http://edcdaac.usgs.gov/modis/dataprod.html for details.

ESDT	temporal resolution	spatial resolution	acquisition range	science quality status
MOD11_L2	daily	1km at nadir	02/24/2000 - March 2004	validated (stage 1) since 06/01/00
MOD11A1	daily	1km at SIN grids	02/24/2000 - March 2004	validated (stage 1) since 06/01/00
MOD11B1	daily	5km at SIN grids	02/24/2000 - March 2004	validated (stage 1) since 06/01/00
MOD11A2	8-day	1km at SIN grids	02/24/2000 - March 2004	based on MOD11A1
MOD11C1	daily	0.05 ° lat/lon grids	currently available at SCF	based on MOD11B1
MOD11C2	8-day	0.05 ° lat/lon grids	currently available at SCF	based on MOD11C1
MOD11C3	monthly	0.05 ° lat/lon grids	currently available at SCF	based on MOD11C1

The V2 daily LST product was validated within 1K with in-situ measurements in 25 clear-sky cases (including 19 cases over land sites) in the LST range of 263-322K and the atmospheric column water vapor range of 0.4-4cm in field campaigns conducted in 2000 -2002 (Wan et al., 2002b; Wan et al., 2004b). The daily LST product was also validated within 0.6K with in-situ measurements in Lake Tahoe in 2000-2001 (Hook at JPL, personal communication).

After the V4 reprocessing was completed for the MODIS data acquired in 2000, we evaluated the calibration accuracies of V4 MODIS TIR data in bands 20, 22, 23, 29, and 31-33 with the in-situ measurement data collected in the June 2000 field campaign in Lake Titicaca, Bolivia, and found that most of the calibration bias values in Tables 4-6 of Wan et al. (2002a) are changed by less than 0:05K and the maximum change is 0.17K for band 33 in the June 13 daytime case. We also compared the V4 LST product with the V2 LST product and validated the V4 LST product with in-situ LST data shown in Table 2 of Wan et al. (2002b). As shown in Table II, the differences between V2 and V4 LST values are less than 0.4K (with a mean difference of less than 0.08K) although there are significant differences between the column water vapor values in V2 and V4 atmospheric profile products (MOD07_02). Therefore, the validation results for V2 and V3 MODIS LST products in the two LST validation papers (Wan et al., 2002b; Wan et al., 2004b)

also apply to the V4 MODIS LST product with uncertainties less than 0.4K.

The V4 Terra MODIS LST product and V3 Aqua MODIS LST product were also validated at accuracies better than 0.6K in the field campaign conducted in Walker Lake, NV, in January 2003, as shown in Table III.

Table II, Comparison between the (V2 and V4) 1km MODIS LSTs and in-situ measured LSTs in validation field campaigns conducted in June - October 2000. The case numbers in Table 2 of Wan et al. (2002b) are kept. V2.5.4 is for all cases except V2.4.3 for case 3 in the V2 column block. Note that the atmospheric column water vapor (cwv) in the upper line comes from MOD07_L2 and that in the lower line comes from radiosonde.

case no.	site	latitude longitude (°)	date (m/d/y) time	view zenith azimuth (°)	in-situ Ts / no. of radiometers / spatial variation (K) (no.) δT_s (K)	atmos. cwv (cm)	V 2 MODIS $T_s(\delta T_s)$ (K)	MODIS -in situ T_s (K)	atmos. cwv (cm)	V 4 LST MODIS - in situ T_s (K)
2	Mono Lake California	37.9930N 118.9646W	7/25/00 11:18 PST	22.09 -79.37	296.01 (3) 0.15	2.1	296.3 (0.2)	+0.3	1.0	296.35 0.34
3	Mono Lake California	38.0105N 118.9695W	10/06/00 11:11 PST	11.35 -78.19	290.17 (4) 0.23	1.4 (0.62)	290.4 (0.1)	+0.2	0.53 (0.62)	290.45 0.28
4	Lake Titicaca Bolivia	16.2470S 68.7230W	6/15/00 15:26 UTC	34.3 -82.7	285.0 (5) 0.3	1.1 (0.29)	285.5 (0.5)	+0.5	0.18 (0.29)	285.73 0.73
7	Bridgeport grassland	38.2202N 119.2693W	7/27/00 22:09 PST	11.81 81.33	281.63 (4) 0.6	1.6	282.4 (0.4)	+0.8	0.64	282.14 0.51
8	Bridgeport grassland	38.2202N 119.2693W	7/29/00 21:57 PST	32.36 77.56	283.24 (4) 0.6	2.4	283.0 (0.2)	-0.2	1.70	282.66 -0.58
9	rice field California	39.5073N 121.8107W	7/27/00 22:10 PST	26.1 77.3	291.20 (1)	1.4	292.1 (0.5)	+0.9	1.63	292.23 1.03
10	rice field California	39.5073N 121.8107W	7/29/00 21:57 PST	42.67 75.8	293.02 (1)	3.0	292.9 (0.8)	-0.1	2.02	292.7 -0.32

Table III, Validation of the V4 Terra MODIS LSTs and V3 Aqua MODIS LSTs with in-situ measured LSTs in January 2003.

case no.	platform	granule ID	date & time (m/d/y) (hh:mm)	viewing zenith angle (°)	atmo. cwv (cm)	in-situ T_s from radiometers (K)	MODIS Ts (δTs) (K)	MODIS - in-situ Ts(K)
1	Terra	A2003018.1845	01/18/03 18:45 UTC	12.2	0.91	279.08	279.64 (0.09)	+0.56
2	Terra	A2003019.0545	01/19/03 05:50 UTC	17.5	1.0	278.93	278.99 (0.16)	+0.06
3	Aqua	A2003019.0955	01/19/03 09:59 UTC	11.4	0.95	278.73	279.05 (0.15)	+0.32
4	Aqua	A2003019.2100	01/19/03 21:04 UTC	5.8	0.91	280.23	280.53 (0.04)	+0.30

Based on the atmospheric temperature and water vapor profiles measured with radiosonde balloons in Railroad Valley, NV in the June 2003 field campaign shown in Table IV and the surface emissivity measured in the field shown in Fig. 4, the radiance-based method was used to validate the V4 Terra and V3 Aqua MODIS LST products. The results are shown in Tables V and VI, respectively. All the LST validation results summarized in Figure 6 indicate that the MODIS LST accuracy is better than 1° C in most clear-sky cases in the range from -10 to 58° C. A series of status reports and the MODIS LST Users' Guide can be found at the MODIS LST home page http://www.icess.ucsb.edu/modis/modis-lst.html site.

Table IV, Atmospheric temperature and water vapor profiles measured in Railroad Valley, NV under clear-sky conditions in June 26-29, 2003.

case no.	date (m/d/y)	start time PDT (hh:mm)	duration (minutes)	height reached (km)	atmos. cwv (cm)	Ts-air (K)
A	6/26/03	10:22	112	16.1	0.71	298.2
B	6/27/03	10:14	103	19.1	0.78	299.7
C	6/27/03	22:58	102	23.2	1.00	291.8
D	6/28/03	02:13	120	23.3	0.90	284.2
E	6/29/03	10:29	120	24.4	0.84	305.2
F	6/29/03	22:05	120	24.3	0.67	291.6

Table V, Radiance-based validation of V4 Terra MODIS LSTs in Railroad Valley, NV. Note that (MS) stands for match score in 1-10.

case no.	granule ID	date & time PDT (m/d hh:mm)	viewing zenith angle (°)	MOD07 cwv, Ts-air (cm, K)	atmos. profile no. (MS)	MODIS LST (K)	ΔT_b in b29 (K)	trans in b31	ΔT_b in b31 (K)
1	A2003177.1800	6/26 11:02	53.7	0.67, 299.3	A (9)	320.18	-0.85	0.88	-1.10
2	A2003178.1840	6/27 11:45	11.5	1.90, 305.2	B (9)	326.78	-0.18	0.92	-0.59
3	A2003179.0545	6/27 22:49	4.6	1.30, 291.8	C (9)	288.43	+0.14	0.91	-0.21
4	A2003180.0630	6/28 23:32	60.2	1.30, 293.4	C (6)	287.82	-0.84	0.84	-0.95
5	A2003180.1830	6/29 10:33	12.0	0.96, 301.4	E (9)	327.62	-0.58	0.92	-0.81
6	A2003181.0535	6/29 22:37	18.4	0.67, 291.6	F (9)	289.86	+0.44	0.93	+0.01

Table VI, Radiance-based validation of V3 Aqua MODIS LSTs in Railroad Valley, NV. Note that (MS) stands for match score in 1-10.

case no.	granule ID	date & time PDT (m/d hh:mm)	viewing zenith angle (°)	MOD07 cwv, Ts-air (cm, K)	atmos. profile no. (MS)	MODIS LST (K)	ΔT_b in b29 (K)	trans in b31	ΔT_b in b31 (K)
1	A2003177.1010	6/26 03:11	46.9	0.64, 287.6	A (7)	280.55	+0.09	0.90	-0.23
2	A2003178.0915	6/27 02:16	40.9	0.61, 288.9	D (6)	280.56	-0.22	0.90	-0.26
3	A2003178:2020	6/27 13:20	44.4	0.56, 298.5	B (8)	331.12	-0.51	0.90	-0.65
4	A2003179.0955	6/28 02:59	31.9	1.01, 289.6	D (9)	281.09	-0.03	0.91	-0.28
5	A2003179.2100	6/28 14:03	26.9	1.29, 290.6	E (6)	331.31	-0.53	0.92	-0.62
6	A2003180.2005	6/29 13:08	55.7	0.80, 302.6	E (8)	326.51	-0.37	0.87	-0.72
7	A2003181.0945	6/30 02:47	11.4	0.50, 289.9	F (8)	282.34	+0.17	0.87	-0.06

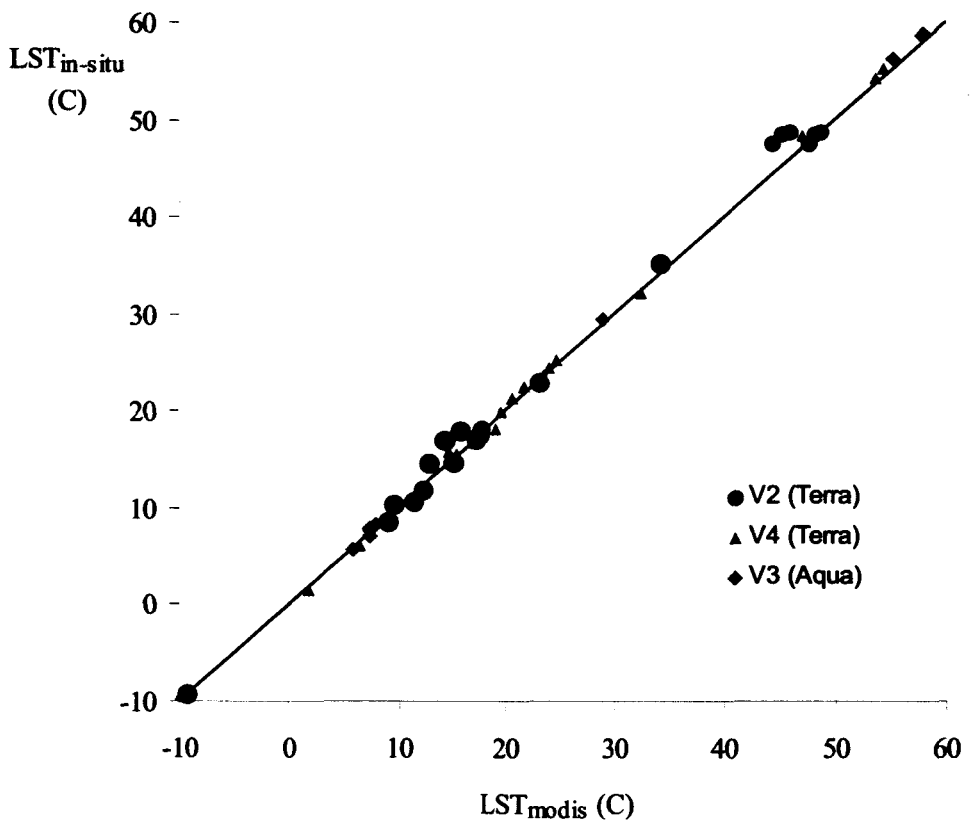

Fig. 6, Comparisons between V2, V3, and V4 MODIS LSTs and in-situ values in field campaigns in 2000-2003.

In Figure 7, the V4 monthly composite MODIS LST product at the 0.05 ° lat/lon CMG grids shows the spatial and seasonal changes in the global LSTs in May-December 2000. Now, more than four years of the V4 MODIS LST products (from 24 February 2000 to the end of March 2004) are available to the public at the EOS Data Gateway for regional and global change studies.

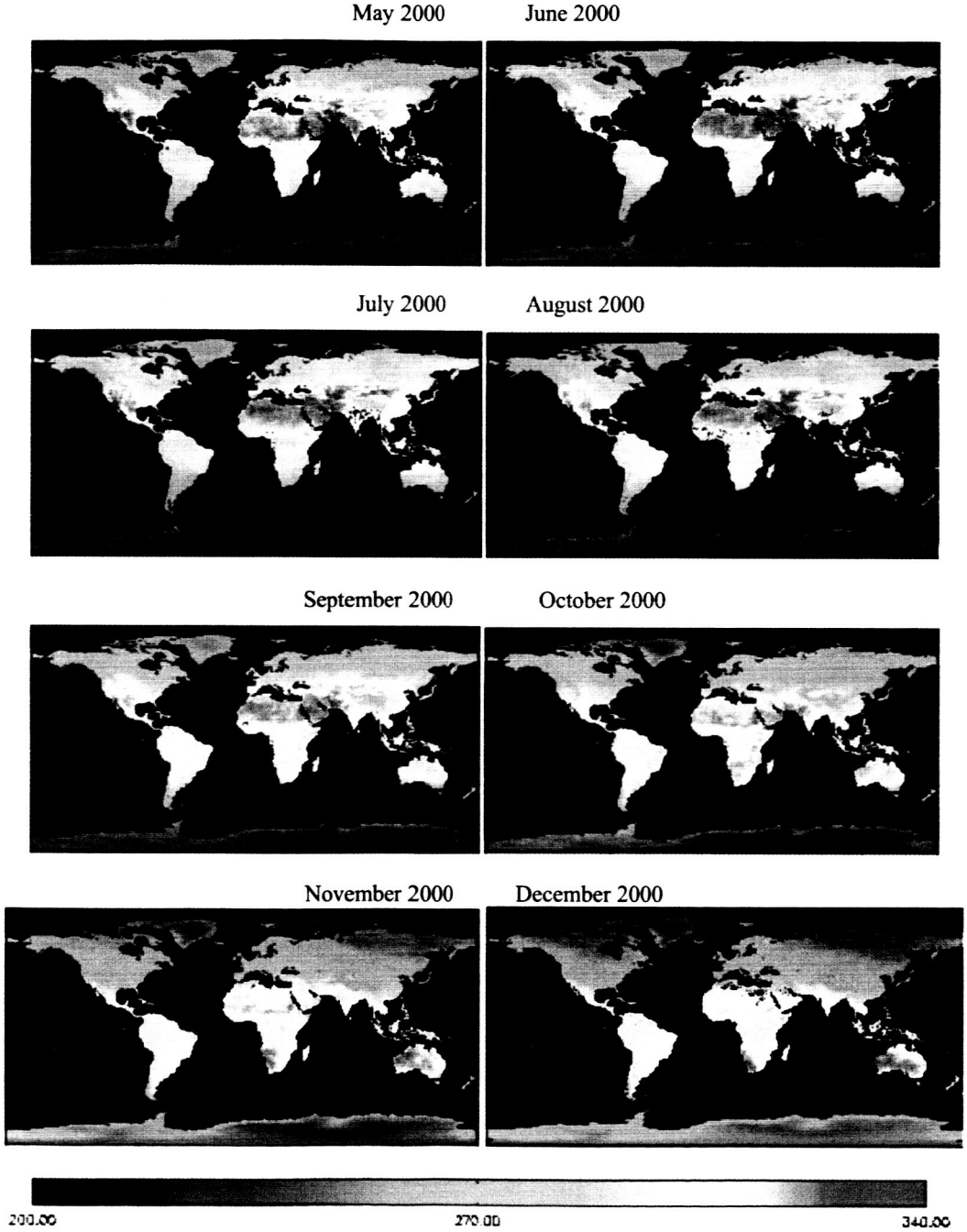

Fig. 7, Monthly global daytime LSTs (K) for May - December 2000.

4. Lessons Learnt

4.1 Cloud-contamination in the MODIS LST Products

In the MODIS LST product, LST is defined by the radiation emitted by the land surface observed by MODIS at the instant viewing angle. The land surface is canopy in vegetated areas or soil surface in bared areas, and whatever objects observed by MODIS thermal infrared (TIR) sensors. One of the basic considerations for the MODIS LST product is to retrieve LST from MODIS TIR data only in clear-sky conditions so that LST is not mixed with cloud-top temperature. As we know, TIR signals cannot penetrate thick clouds, it is difficult to correct the effect of thin clouds on the TIR signals without knowing the exact optical depth of thin clouds, and the probability of cloudy conditions is often larger than 50% at the regional and global scales. Therefore, cloudy pixels must be skipped in the LST processing (giving a fillvalue, zero, LST to cloudy pixels). The LST retrieval in a MODIS swath is constrained to land and inland water pixels that have nominal Level 1B radiance values, are in clear-sky conditions at a 99% confidence defined in the MODIS cloud-mask product (MOD35). In the V4 LST processing, LST retrieval is made for lake and river pixels at clear-sky conditions with a 66% and higher confidence defined in MOD35 and for other land pixels in clear-sky at a 99% confidence, in order to improve the consistency between the spatial LST distributions over lakes and their surrounding lands in most cases.

It has been a known issue that there are cloud-contaminated LSTs in the MODIS LST product. Although the state-of-art techniques based on multiple MODIS bands have been used in the MODIS cloud mask product (MOD35_L2), and the MODIS LST PGE produces LSTs only for the clear-sky land pixels at the highest confidence (99%) defined by MOD35_L2, there are still some possibilities that MODIS LSTs are contaminated with cloud effects because of the difficulty to accurately discriminate true clear-sky pixels from cloud pixels and pixels contaminated with sub-pixel clouds. There have been more problems with MOD35_L2 over inland lakes, and in semi-arid and arid regions. We made feedbacks to the MODIS Cloud Mask Group at the University of Wisconsin since mid 2000.

A double-screen scheme (Wan et al., 2002b) has been used to remove the cloud-contaminated LSTs in the extreme conditions at the global scale in the generation of the daily global LST product at 0.05 degree climate model grids (CMG). For individual pixel and grid at a given location, we developed another cloud-screen scheme to remove cloud-contaminated LSTs in the MODIS LST level-2 (MOD11_L2) and level-3 (MOD11A1, MOD11A2, and MOD11B1). We define a target grid (or pixel) with its center at the given latitude/longitude location and its size equal to the nearby grid (or pixel). The LST value for the target grid at homogeneous sites can be

interpolated from the values of its four surrounding grids. With constraints on spatial and temporal variations in LSTs, the cloud-screen scheme consists of three options (with user-defined N, $(\Delta T)_S$ and $(\Delta T)_T$) to remove cloud-contaminated LSTs:

A. non-fillvalue LST exists at less than N grids.

B. the maximum difference between the LST values at these grids is larger than $(\Delta T)_S$.

C. step 1: remove worst LSTs in the time sequence of LSTs if its difference from the 32-day maximum value is larger than 4 times $(\Delta T)_T$ or its difference from the 16-day maximum value is larger than 3 times $(\Delta T)_T$, and then calculate 8-day averaged values;

step 2: remove LSTs if its difference from the 8-day averaged value is larger than $(\Delta T)_T$.

We evaluated the cloud-screen scheme in large lakes first because in-situ and satellite data indicate that the surface temperature in large lakes is quite homogeneous spatially and varies with time slowly (Irbe, 1992; Malm and Jönsson, 1994; Malm and Zilitinkevich, 1994). Lake Tahoe spans California and Nevada at elevation of 1987m above sea level, with a size of 35km long, 19km wide, and average depth of 488m, not freezing around the year. Namco (lake) in Tibet is at elevation of 4530m above sea level, about 80km long and 50km wide, average depth of 40m, freezing in the winter. If any LST value in Lake Tahoe is below the freezing point, 273.15K, it is definitely cloud-contaminated. And similarly for the LST value in Namco in the non-freezing seasons. This scheme is applied to the V3 and V4 1km MODIS LST (MOD11A1) products in Lake Tahoe and Namco in 2002 to show the impact of using the MODIS cloudmask (MOD35) product in different ways: processing lake and river pixels only in clear-sky condition at the 99% confidence level in V3 and at equal to or larger than the 66% confidence level in V4. The results are shown in Table VII. The number in parentheses is the number of days when the MODIS data are available. A location near the centers of Lake Tahoe and Namco is selected. In the first row of the table body, N = 1 without $(\Delta T)_S$ and $(\Delta T)_T$ options means that only the grid covering the target point is considered, there are 174 days and 39 nights with non-fillvalue LSTs in Lake Tahoe in totally 351 days in 2002 when V3 MOD11A1 product is available. The V4 MOD11A1 product is available for 355 days. There are 257 days and 202 nights with non-fillvalue LSTs. The daytime and nighttime LSTs in V3 and V4 are shown in the top plot of Figure 8. One nighttime LST in V3 (where all LST pixels in clear-sky conditions at the 99% confidence level defined by MOD35) is around 264K. And there are more daytime and nighttime LSTs below 273.15K in V4. As shown in the second row of Table VII, N = 4 means that the LST will be removed as cloud-contaminated value if any grid in the four neighboring grids is in cloudy

conditions (with fillvalue for LST). In the third row, N = 4 and a spatial variation constraint of $(\Delta T)_S$ = 3.0K is applied. In the fourth row, N = 4 and both spatial and temporal constraints of 3.0K are applied. After applying the cloud-screen scheme with these options, the daytime and nighttime LSTs are above 273.15K as shown in the bottom plot of Figure 8. Similarly, the results for Namco (at 4530m above sea level) are shown in the right side of Table VII and Figure 9. The top plot indicates that the daytime and nighttime LSTs in V3 and V4 spread in a wide range from 230K to 290K. It is obvious that the lake surface temperature could not change so much in a few days. This plot clearly indicates that the current MODIS cloudmask does not work well in high elevation conditions. After applying the cloud-screen scheme with N = 4 and spatial and temporal constraints of 3K, the V4 daytime and nighttime LSTs are shown in the bottom plot of Figure 9. The time sequence of the LSTs clearly shows the days of freezing and lake-ice melting in Namco (the horizontal dash line presents freezing temperature of 273.15K).

Table VII, The change in number of LSTs at one point in Lake Tahoe and Namco (lake) in the V3 and V4 1km MODIS LST (MOD11A1) products in 2002 after applying the cloud-screen scheme with constraints on spatial and temporal variations.

N	$(\delta T)_S$	$(\delta T)_T$	Lake Tahoe (39.101 ° N, 120.04 ° W)				Namco (30.69 ° N, 90.53 ° E)			
			in V3		in V4		in V3		in V4	
			day	night	day	night	day	night	Day	night
1			174 (351)	39 (351)	257 (355)	202 (355)	170 (353)	102 (353)	219 (355)	223 (355)
4			162	10	250	191	163	66	200	210
4	3.0		162	10	249	187	160	65	193	177
4	3.0	3.0	159	10	240	184	156	47	177	135
1		3.0	169	39	245	195	163	76	190	138

Comparing the numbers of LSTs in the first row and the fourth row (219 vs 177 for V4 daytime LSTs and 223 vs 135 for V4 nighttime LSTs) indicates that the cloud-contaminated LSTs account for about 20% in daytime and 40% in nighttime. There is a trade-off in choosing the values for the spatial and temporal variation constraints. The smaller the values, the stronger the constraints, thus more LSTs will be removed. If the constraints are too strong, some really clear-sky LSTs may be also removed. If the constraints are too weak, some really cloud-contaminated LSTs cannot be removed. Test indicates that a reasonable constraint value can be selected in the range of 2-4K for large lakes. In the last row of Table VII, N = 1 and only a temporal constraint

of 3K is applied. This option should be used near ocean and lake coastal lines, and in lands where the spatial variation in LSTs is large because near boundaries of different land types. This option works fine in the cases of Lake Tahoe and Namco as long as there are enough points in the time sequence of LSTs. The V3 nighttime LST around 264K in Lake Tahoe cannot be removed by the temporal option alone because it is the only nighttime LST in the first four months in V3.

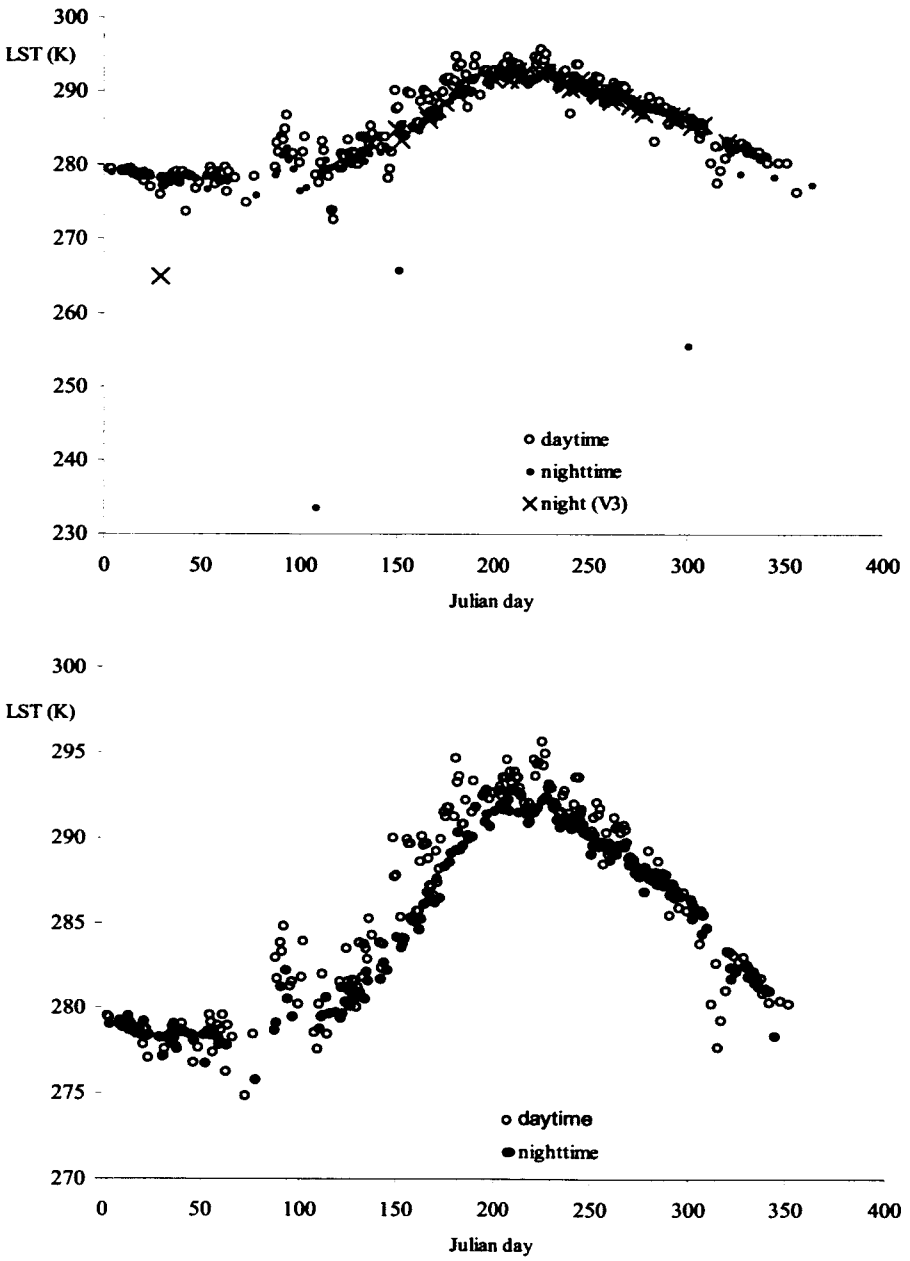

Fig. 8, The daytime and nighttime LSTs near the center of Lake Tahoe in the V3 and V4 MOD11A1 products in 2002 before (top) and after (bottom) applying the cloud-screen scheme.

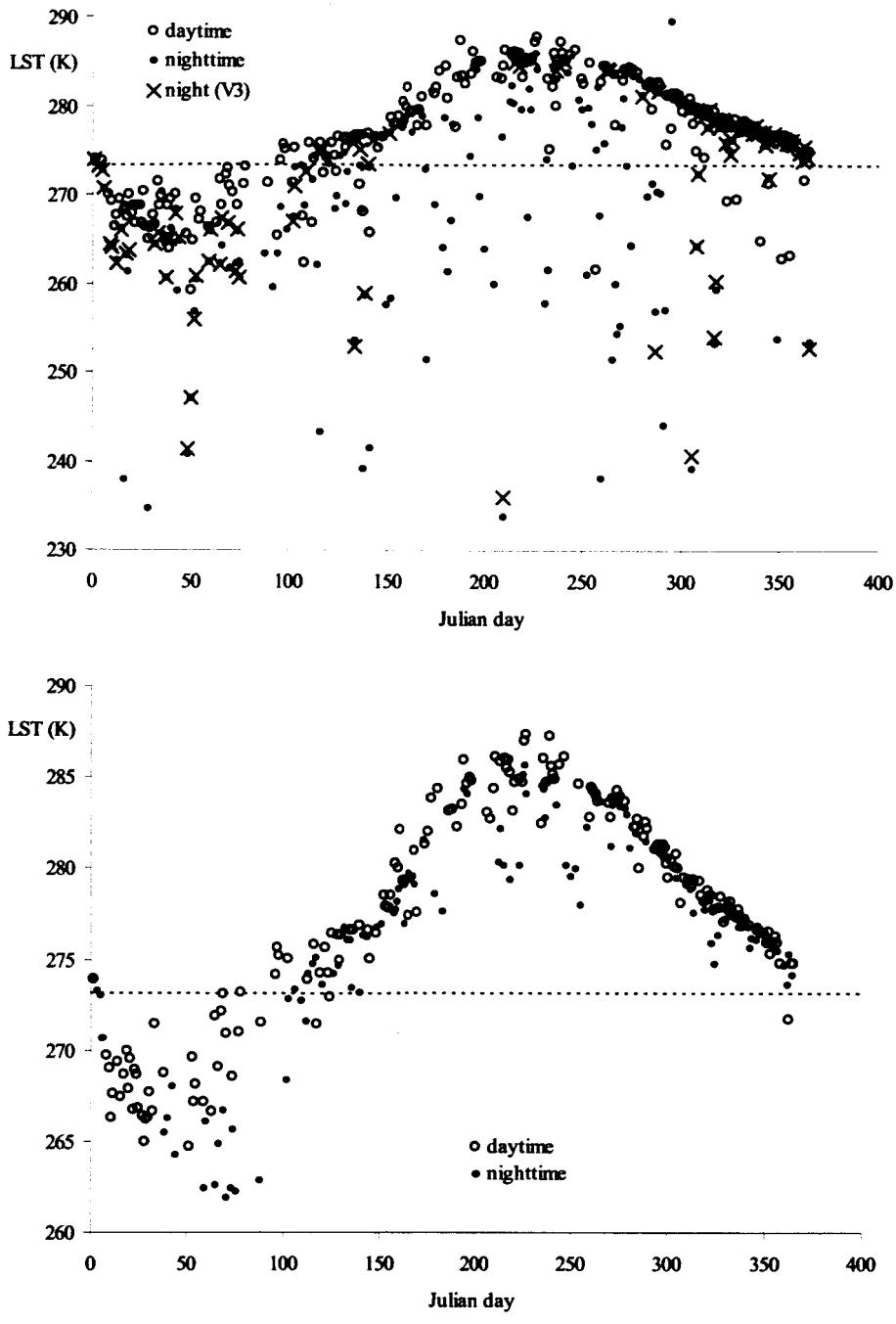

Fig. 9, The daytime and nighttime LSTs at 30.69°N, 90.53 °E in Namco (lake) in the V3 and V4 MOD11A1 products in 2002 before (top) and after (bottom) applying the cloud-screen scheme. Note the horizontal line at 273.15K in both plots.

The cloud-screen scheme is also applied to the V4 5km MODIS LST (MOD11B1) product in 2003 at test sites in lakes, snow/ice, and semi-arid regions. The results are shown in Table VIII. Considering the different years and the different grid sizes in MOD11A1 (1km) and MOD11B1 (5km), the numbers of LSTs in the Lake Tahoe and Namco cases before and after applying the cloud-screen scheme are different but they are comparable. Besides Lake Tahoe and Namco (lake), we also applied the cloud-screen scheme to the MOD11B1 product in 2003 at latitude 47.25°N and longitude 87.22°W in the middle of Lake Superior, Michigan. According to CTV.ca News on 11 March 2003 titled "Great Lakes Article: Great Lakes freeze delays shipping season" (http://www.greatlakesdirectory.org/on/031103_great_lakes.htm), "For the first time in years, three of the Great Lakes (Lake Superior, Lake Huron, and Lake Erie) have frozen over shoreline-to-shoreline." Lake Erie, the shallowest of the lakes, often freezes from shore to shore. But Superior and Huron are both among the world's five largest lakes, and don't freeze over often because their enormous volumes of water rarely get cold enough. Before applying the cloud-screen scheme, the daytime and nighttime LSTs in the MOD11B1 product are shown in the top plot of Figure 10. We can see that there are several LSTs below 273.15K in the non-freezing season (approximately after Julian days 120). The values of parameters N, $(\Delta T)_S$ and $(\Delta T)_T$ in applying the cloud-screen scheme to this case are 4, 3K, and 5K before Julian 121, and 4, 3K, and 3K starting from Julian day 121, respectively. If we use the same parameters (4, 3K, 3K) for the whole year, three daytime LSTs and three nighttime LSTs below 268K (in the bottom plot) would be removed. These six LST values seem reasonable for the lake ice in the cold spring. Note that the numbers of LSTs are given in the parentheses only in the figures. Different values are used in the spatial and temporal constraints on daytime and nighttime LSTs at the snow/ice site in Greenland, and at Gaize in the semi-arid region in Tibet.

The daytime and nighttime LSTs at a snow/ice site (63.0°N, 47.8°W) in Greenland in 2003 are shown in Figure 11. There is no daytime LST in the first 50 days and last 60 days of the year, and no nighttime LST in the first 50 days and last 30 days because of the two requirements in the day/night LST algorithm: solar zenith angle cannot be larger than 65° and the time difference in the pair of day and night MODIS observations cannot be larger than 32 days. Before applying the cloud-screen scheme, the daytime and nighttime LSTs shown in the top plot of Figure 11 are not well separated, and some nighttime LST values are too low in the summer. After applying the scheme, the daytime LSTs are well separated from nighttime LSTs and there are daytime LSTs within 273.15 ± 1K in the period of Julian days from 150-240. This time sequence of daytime LSTs clearly shows the snow/ice melting season in Greenland. There is no daytime LST larger

than 274.15K at the snow/ice site, indicating that the accuracy of the LSTs at the snow/ice site in the MOD11B1 product is better than 1K. The cloud-screen scheme is also validated in the comparison between MODIS LST data and ground-based measurement data at the Gaize automatic weather station (32.3°N, 84.06°E, 4420m above sea level) in the western Tibet plateau (Wang, personal communication). The numbers in Table VIII indicate that the cloud-contaminated LSTs account for about 30% in daytime and 10% in nighttime at the Gaize site.

Table VIII, The change in number of LSTs at one point in each test site in the V4 5km MODIS LST (MOD11B1) products in 2003 after applying the cloud-screen scheme with constraints on spatial and temporal variations.

N	$(\delta T)_S$	$(\delta T)_T$	39.101°N, 120.04°W in Lake Tahoe		30.69°N, 90.53°E in Namco		63.0°N, 47.8°W in Greenland		32.3°N, 84.06°E in Gaize, Tibet	
			day	night	day	night	day	night	day	night
4			264 (256)	291 (356)	196 (356)	193 (356)	145 (356)	174 (356)	246 (356)	216 (356)
4	3.0		242	231	160	144				
4	3.0	3.0	230	221	151	132				
4	3.0						121	121		
4	3.0	4.0					103	81		
4	5.0								181	
4	5.0	10.0							178	
4	4.0									193
4	4.0	8.0								193

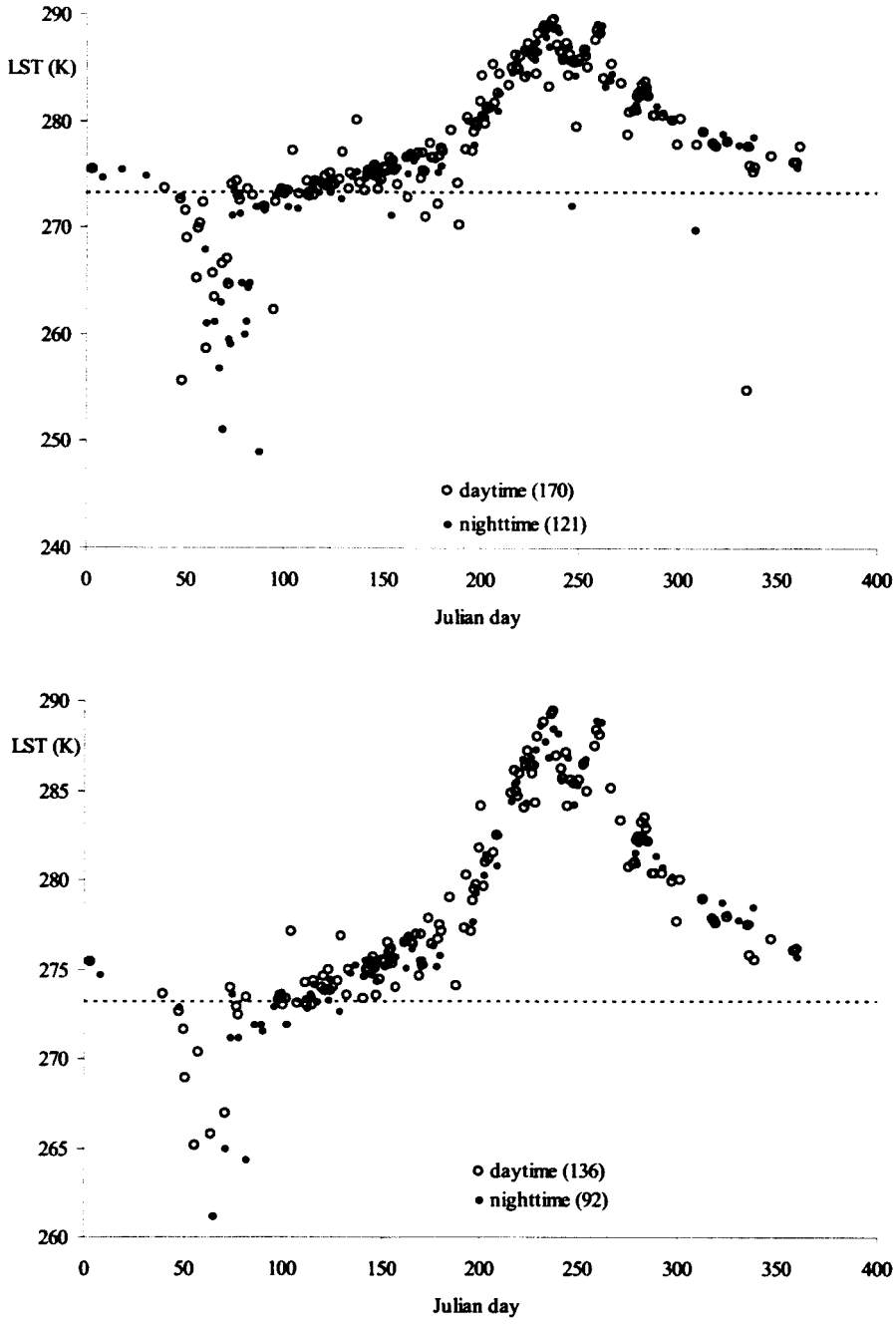

Fig. 10, The daytime and nighttime LSTs at 47.25° N, 87.22° W in Lake Superior in V4 MOD11B1 in 2003 before (top) and after (bottom) applying the cloud-screen scheme. Note the horizontal line at 273.15K in both plots.

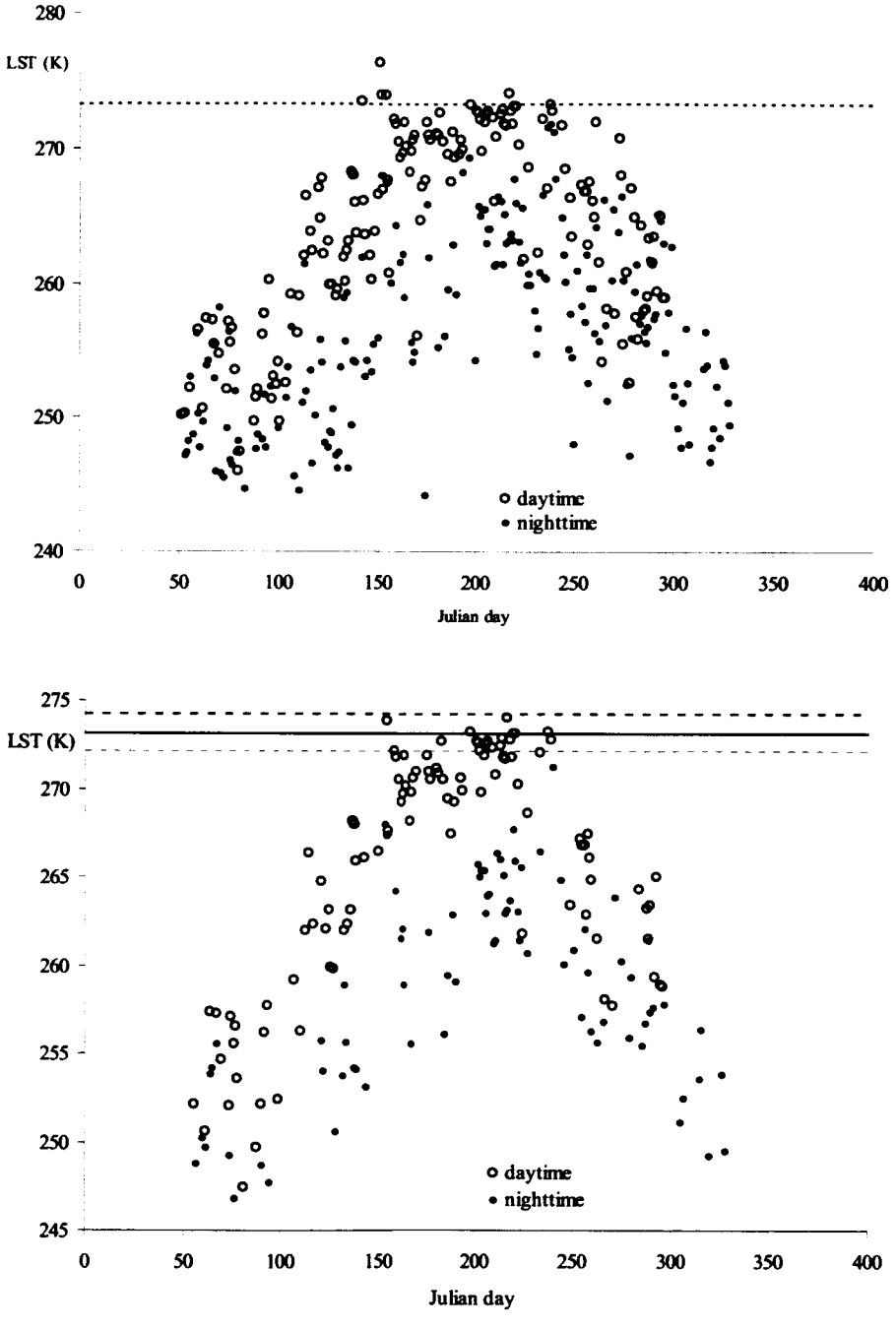

Fig. 11, The daytime and nighttime LSTs at 63.0°N, 47.8°W in Greenland in the V4 MOD11B1 product in 2003 before (top) and after (bottom) applying the cloud-screen scheme. Note the horizontal line at 273.15K in both plots and two more lines in the bottom plot, one at 272.15K and another at 274.15K.

Similarly, the cloud-screen scheme was used for MOD11A1 and MOD11B1 products in 2001-2003 over a site in Amazon rain forest. As shown in Table IX, the number of clear-sky days is quite small especially for nighttime observations in this tropical region.

Table IX, The change in number of LSTs at 5.0°S, 65.0°W in Amazon rain forest in V4 1km and 5km MODIS LST (MOD11A1 and MOD11B1) products in 2001-2003 after applying the cloud-screen scheme with constraints on spatial and temporal variations.

N	$(\delta T)_S$	$(\delta T)_T$	2001				2002				2003			
			MOD11A1		MOD11B1		MOD11A1		MOD11B1		MOD11A1		MOD11B1	
			day	night	day	night	day	night	day	night	day	night	day	night
3			53	15	74	29	65	16	77	36	62	22	71	30
3	3.0		53	15	62	18	65	16	62	25	62	22	69	30
3	3.0	3.0	45	15	60	18	57	16	58	25	56	20	67	29

Although the cloud-contaminated LSTs in the MOD11A1 and MOD11B1 products can be removed with the cloud-screen scheme, it will hold the release of daily MODIS LST products for more than 32 days. Users would not like such long delay. It would also be a big problem for the MODIS product generation system to stage the daily LST products for so many days for the cloud-screen post-processing. The best approach is to do a good job from the beginning. It requires a significant improvement of the current MODIS cloudmask product. In the generation of the current MODIS cloudmask product, the spectral tests in ocean and inland water use the same thresholds. The variations in land surface elevation and emissivities are not considered in the thresholds for land. In order to improve the MODIS cloudmask product, smart thresholds, which depend on land surface elevation and thermal properties, may be needed.

The V4 CMG LST (MOD11C series) products were also generated with the MODIS LST SCF at UCSB from all the V4 MOD11B1 data in acquisition range from 2000-2003 with the cloud-screen scheme removing cloud-contaminated LSTs.

4.2, Indirect Validation of the 5km MODIS LST product

Our multi-year experience of in-situ LST measurements over land sites indicates that it is not easy to obtain reliable averaged LST values over a 1km grid with multiple TIR radiometers, especially during the daytime. It is more difficult to obtain accurate LST values over a 5km grid

from ground-based measurements for the validation of the 5km LST product (MOD11B1). Therefore, it is more practical to indirectly validate the 5km LST product (MOD11B1) through comparing the LSTs in MOD11B1 to the LSTs in MOD11A1 (the 1km LST product) aggregated over 5km grids. Note that the aggregated LST values are also kept in the MOD11B1 product. After the severely and moderately cloud-contaminated LSTs are removed by the cloud-screen scheme, we made such comparisons at test sites in lakes, snow/ice, Amazon rain forest and semi-arid regions in the MODIS LST products in 2003. The mean and standard deviation (std dev) values of the differences are shown in Table X.

Table X, The mean and standard deviation values of the differences (LST values in MOD11A1 minus the LST values in MOD11B1) after applying the cloud-screen scheme at test sites in lakes, snow/ice, Amazon rain forest and semi-arid regions in 2003.

site	lat, lon (°)	difference in daytime LSTs (K)		difference in nighttime LSTs (K)		difference in day/night LSTs (K)	
		mean	std dev	mean	std dev	mean	std dev
Lake Superior, MI	47.25, -87.22	0.02	0.54	0.06	0.55	0.03	0.55
Lake Tahoe, CA	39.101, -120.04	-0.05	0.53	0.07	0.58	0.01	0.56
Namco (lake), Tibet	30.69, 90.53	0.22	0.58	0.41	0.55	0.31	0.58
Namco ($T_s > 0°C$)	30.69, 90.53	0.21	0.58	0.32	0.56	0.26	0.57
Greenland (snow/ice)	63.0, -47.8	-0.48	0.75	-0.37	1.11	-0.44	0.97
Greenland (T_s>260K)	63.0, -47.8	-0.27	0.73	0.002	1.05	-0.18	0.88
Amazon (rain forest)	-5.0, -65.0	-1.28	0.66	-1.38	0.51	-1.31	0.62
Gaize, Tibet (semi-arid)	32.30, 84.06	-1.89	0.70	-1.62	0.65	-1.75	0.68

The differences in daytime LSTs are slightly different from the differences in nighttime LSTs. The last two columns show the mean and std dev of the differences in daytime and nighttime LSTs combined together. There are three major factors behind the differences: (1) errors in the classification-based emissivities in bands 31 and 32 used in the split-window algorithm to retrieve the LSTs in MOD11A1, (2) the 5km LSTs in MOD11B1 are retrieved by the day/night method that is significantly different from the split-window method; and (3) the effects of remaining

weak cloud-contaminations in LSTs may depend on grid sizes, the retrieval methods, and surface elevation. More research work is required to evaluate these factors. In cases of Lake Superior and Lake Tahoe, the mean difference and std dev values are less than 0.04K and 0.57K. In case of Namco, the mean difference is about 0.3K and the std dev value is slightly larger. In the case of Greenland site, the mean difference depends on the LST region. This indicates that the errors in the classification-based emissivities may be different for snow and ice. In the cases of test sites in Greenland, Amazon rain forest and the semi-arid site in Gaize, Tibet, the mean differences are all negative values, indicating the band emissivities used in the split-window algorithm are overestimated in most land-cover types, especially in semi-arid and arid regions. The details of comparisons in all these cases but the Amazon site are shown in Figures 12-14. We have less confidence in the Amazon case because of the persistent clouds in the tropical region.

Although more investigation is required for the validation of the 5km MODIS LST product, the consistent correlations in the wide temperature regions at different sites shown in Table X and Figures 12-14 indicate that the 5km LSTs in MOD11B1 retrieved by the day/night method are reliable and their quality is very good. The good agreement between the retrieved surface emissivities over the Sahara Desert and those measured from sand samples in the laboratory, and the good agreement between the retrieved surface emissivities in Caspian Sea and the theoretical emissivity values of sea water (Wan et al, 2004b), are the examples for indirect validations of retrieved emissivities in the MOD11B1 product. We plan to validate the retrieved surface emissivities in the MOD11B1 product in large homogeneous grasslands and make comprehensive analysis of the correlations between surface emissivities and land cover types in the near future. The classification-based emissivity look-up table used in the generalized split-window algorithm will be updated with the surface emissivities retrieved from MODIS data.

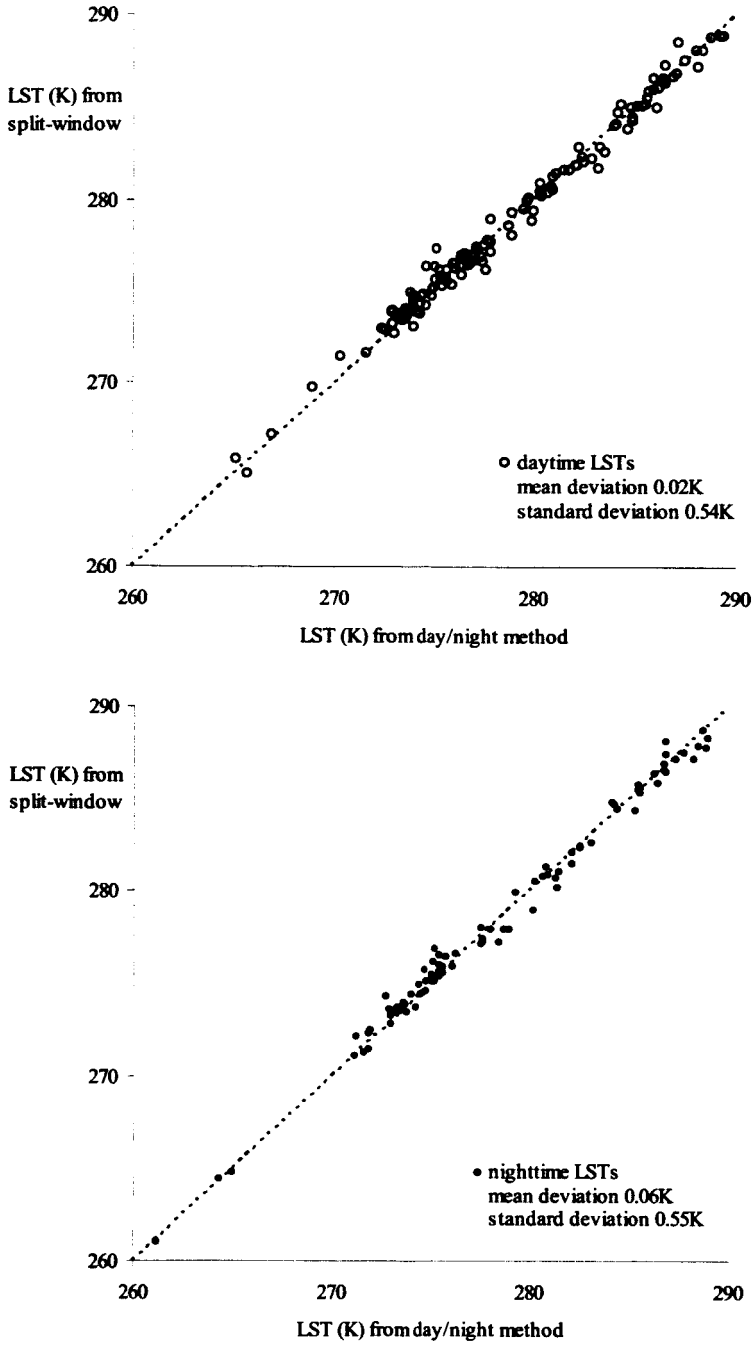

Fig. 12, Comparison between the LSTs retrieved by the split-window method and the day/night method in the V4 MOD11B1 product in 2003 in Lake Superior in day (top) and night (bottom).

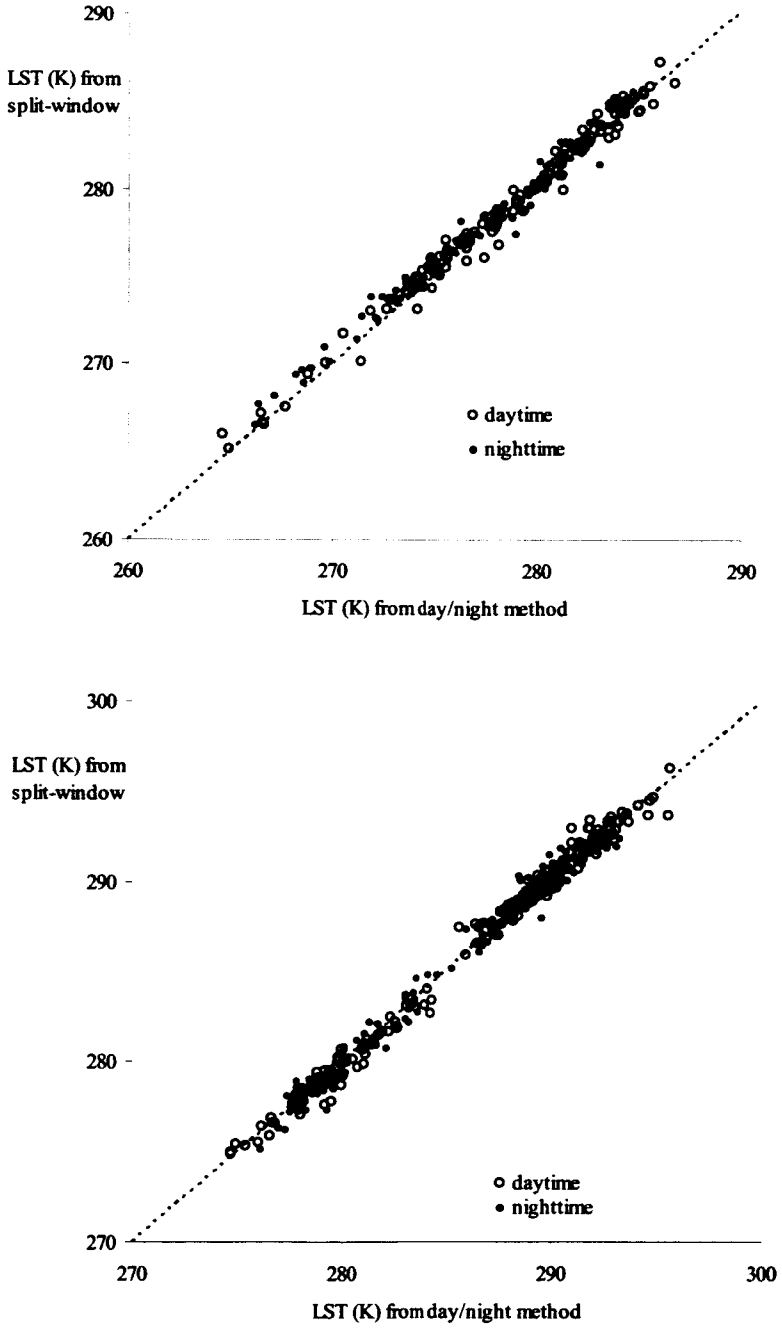

Fig. 13, Comparison between the LSTs retrieved by the split-window method and the day/night method in the V4 MOD11B1 product in 2003 in Namco, Tibet (top) and Lake Tahoe (bottom).

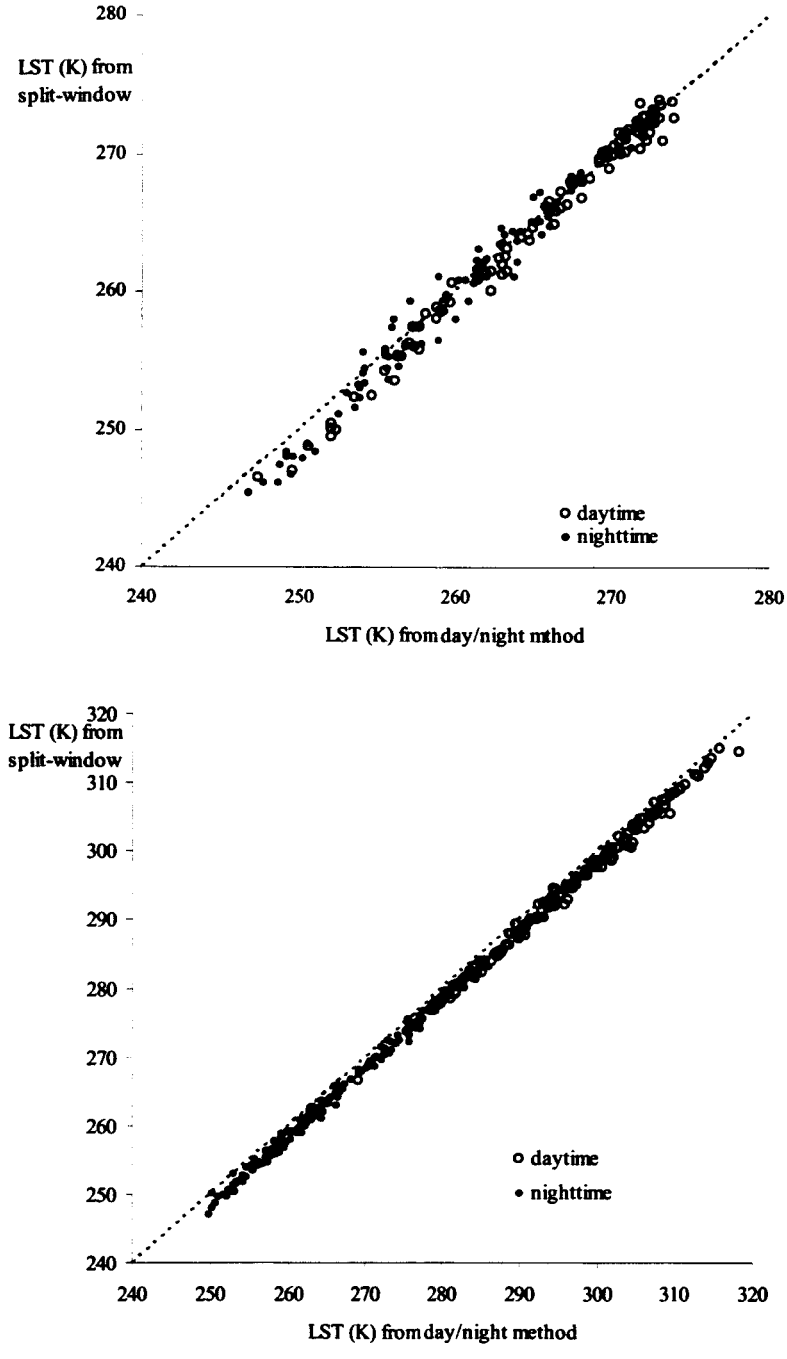

Fig. 14, Comparison between the LSTs retrieved by the split-window method and the day/night method in the V4 MOD11B1 product in 2003 in Greenland (top) and at Gaize, Tibet (bottom).

5. Examples of MODIS LST Applications

The MODIS LST product has been used as input in the generation of MODIS Land-Cover (MOD12Q1) and Surface Evapotranspiration (MOD16) products. The LST and surface emissivity data in the MODIS LST products have been used in Common Land Model studies at NCAR, NASA GSFC, and universities (Jin and Dickinson, 1999; Jin, personal communication, 2003). It was used by http://earthobservatory.nasa.gov/Newsroom to show special weather events such as the unusually warm 2001-02 winter in the contiguous United States, the severe winter storm that swept across the Mexico state of Michoan in January 2002 leaving hundreds of million Monarch butterflies dead on their wintering grounds, and the record heat wave in the central Europe in July 2003. The MODIS LST product was also used in drought monitoring (Wan et al., 2004a), assessment of fire risk, and predicting riparian evapotranspiration (Nagler, personal communication, 2004). As shown in Figures 9-11, the multi-year MODIS LST product may be used to monitor snow/ice melting, lake freezing, and lake ice melting in climate studies at global and regional scales.

6. Related Publications

Z. Wan, Y. Zhang, Q. Zhang, and Z.-L. Li, "Quality assessment and validation of the MODIS global surface temperature", *Int. J. Remote Sens.*, 25, 261-274 (2004).

Z. Wan, P. Wang, and X. Li, "Using MODIS land surface temperature and normalized difference vegetation index for monitoring drought in the southern Great Plains, USA", *Int. J. Remote Sens.*, 25, 61-72 (2004).

Z. Wan, Y. Zhang, Q. Zhang, and Z.-L. Li, "Validation of the land-surface temperature products retrieved from Terra Moderate Resolution Imaging Spectroradiometer data," *Remote Sens. Environ.*, 83, 163-180 (2002).

Z. Wan, "Monitoring thermal status of ecosystems with MODIS land-surface temperature and vegetation index products," *Remote Sensing for Agriculture, Ecosystems, and Hydrology IV, Proc. SPIE* , 4879, 280-288 (2002).

Z. Wan, "Estimate of noise and systematic error in early thermal infrared data of the Moderate Resolution Imaging Spectroradiometer (MODIS)," *Remote Sens. Environ.*, 80, 47-54 (2002).

Z. Wan, Y. Zhang, Z.-L. Li, R. Wang, V.V. Salomonson, A. Yves, R. Bosseno, and J. F. Hanocq, "Preliminary estimate of calibration of the Moderate Resolution Imaging Spectroradiometer (MODIS) thermal infrared data using Lake Titicaca," *Remote Sens. Environ.*, 80, 497-515 (2002).

X.-L. Ma, Z. Wan, C.C. Moeller, W.P. Menzel, and L.E. Gumley, "Simultaneous retrieval of atmospheric profiles, land-surface temperature, and surface emissivity from Moderate Resolution

Imaging Spectroradiometer thermal infrared data: extension of a two-step physical algorithm," *Appl. Optics.*, 41, 909-924 (2002).

X.-L. Ma, Z. Wan, C.C. Moeller, W.P. Menzel, L.E. Gumley, and Y. Zhang, "Retrieval of geophysical parameters from Moderate Resolution Imaging Spectroradiometer thermal infrared data: evaluation of a two-step physical algorithm," *Appl. Optics.*, 39, 3537-3550 (2000).

Z. Wan, Y. Zhang, X. Ma, M.D. Kig, J.S. Myers, and X. Li, "Vicarious calibration of the Moderate-Resolution Imaging Spectroradiometer Airborne Simulator (MAS) thermal-infrared channels," *Appl. Optics.*, 38, 6294-6306 (1999).

Z.-L. Li, F. Becker, M.P. Stoll, Z. Wan, and Y. Zhang, "Channel selection for soil spectrum reconstruction in 8-13 μm region," *J. Geophys. Res. - Atmos.*, 104, 22271-22285 (1999).

Z.-L. Li, F. Becker, M.P. Stoll, and Z. Wan, "Evaluation of six methods for extracting relative emissivity spectra from thermal infrared images," *Remote Sens. Environ.*, 69, 197-214 (1999).

C. Justice, E. Vermote, J. R. G. Townshend, R. Defries, D. P. Roy, D.K. Hall, V. V. Salomonson, J. Privette, G. Riggs, A. Strahler, W. Lucht, R. Myneni, Y. Knjazihhin, S. Running, R. Nemani, Z. Wan, A. Huete, W. van Leeuwen, R. Wolfe, L. Giglio, J-P. Muller, P. Lewis, and M. Barnsley, "The Moderate Resolution Imaging Spectroradiometer (MODIS): Land remote sensing for global change research," *IEEE Trans. Geosci. Remote Sens.*, 36, 1228-1249 (1998).

Z. Wan, Y.-Z. Feng, Y. Zhang, and M. D. King, "Land-surface temperature and emissivity retrieval from MODIS Airborne Simulator (MAS) Data," *Summaries of the Seventh JPL Airborne Earth Science Workshop, January 12-16, 1998, JPL Publication 97-21.*, vol. 3, 57-66 (1998).

W. Snyder, Z. Wan, Y. Zhang, and Feng, Y.-Z. Feng, "Classification-based emissivity for land surface temperature measurement from space," *Int. J. Remote Sens* , 19, 2753-2774 (1998).

W. Snyder and Z. Wan, "BRDF models to predict spectral reflectance and emissivity in the infrared," *IEEE Trans. Geosci. Remote Sens.*, 36, 214-225 (1998).

W. Snyder, Z. Wan and X. Li, "Thermodynamic constraints on reflectance reciprocity and Kirchhoff's law," *Appl. Optics.*, 37, 3464-3470 (1998).

Z. Wan and Z.-L. Li, "A Physics-Based Algorithm for Retrieving Land-Surface Emissivity and Temperature from EOS/MODIS Data," *IEEE Trans. Geosci. Remote Sens.*, 35, 980-996 (1997).

W. Snyder, Z. Wan, Y. Zhang, and Y.-Z. Feng, "Thermal Infrared (3-14 microns) Bidirectional Reflection Measurements of Sands and Soils," *Remote Sens. Environ.*, 60, 101-109 (1997).

W. Snyder, Z. Wan, Y. Zhang, and Y.-Z. Feng, "Requirements for Satellite Land Surface Temperature Validation Using a Silt Playa," *Remote Sens. Environ.*, 61, 279-289 (1997).

W. Snyder and Z. Wan, "Surface Temperature Correction from Active Infrared Reflectance Measurements of Natural Materials," *Appl. Optics*, 35, 2216-2220 (1996).

Z. Wan and J. Dozier, "A Generalized Split-Window Algorithm for Retrieving Land-Surface Temperature from Space," *IEEE Trans. Geosci. Remote Sens.*, 34, 892-905 (1996).

S. W. Running, C. O. Justice, V. Salomonson, D. Hall, J. Barker, Y. Kaufman, A. Strahler, A. Huete, J.-P. Muller, V. Vanderbilt, Z. Wan, and P. Teillet, "Terrestrial remote sensing science and algorithms planned for EOS MODIS," *Int. J. Remote Sens.*, 15, 3587-3620 (1994).

J. Dozier and Z. Wan, "Development of Practical Multiband Algorithms for Estimating Land Surface Temperature from EOS/MODIS data," *Adv. Space Res.*, 14, 381-389 (1994).

Z. Wan, D. Ng and J. Dozier, "Spectral emissivity measurements of land-surface materials and related radiative transfer simulations," *Adv. Space Res.* , 14, 81-90 (1994).

7. Conclusions

The UCSB MODIS LST Group successfully completed the work in NASA Contract NAS5-31370. We developed MODIS LST ATBD, two LST algorithms, the PGE codes for Terra and Aqua MODIS LST products, TIR instrumentation and calibration procedures. Three vicarious calibration field campaigns were conducted to evaluate the accuracies of MODIS TIR bands. Four to six field campaigns were conducted each year since 2000 to validate the daily MODIS LST products. The 1km MODIS LST accuracy is better than 1° C in most clear-sky cases in wide ranges of the LST and atmospheric conditions. Cloud-screening schemes were developed to remove the LSTs contaminated by the cloud effects severely and moderately from the long time sequence of daily 1km and 5km LST products. The 5km LST product (MOD11B1) was indirectly validated through comparisons to the 1km LST product at a series of sites with multi-year data.

Acknowledgements

This work was supported by EOS Program contract NAS5-31370 of the National Aeronautics and Space Administration. Drs. William Snyder, Zhao-liang Li, Yue-zhong Feng, Ruibo Wang, Pengxin Wang, Qincheng Zhang, Yulin Zhang, and Xia-lin Ma participated in this work in different time periods.

REFRENCES

Becker, F., "The impact of spectral emissivity on the measurement of land surface temperature from a satellite," *Int. J. Remote Sens.*, vol. 8, no. 10, pp. 1509-1522, 1987.

Becker, F. and Z.-L. Li, "Temperature-independent spectral indices in thermal infrared bands," *Remote Sens. Environ.*, vol. 32, no. 1, pp. 17-33, 1990a.

Becker, F. and Z.-L. Li, "Toward a local split window method over land surface," *Int. J. Remote Sens.*, vol. 11, no. 3, pp. 369-393, 1990b.

Berk, A., G. P. Anderson, L.S. Bemstein, P. K. Acharya, H. Dothe, M. W. Matthew, S. M. Adler-Golden, J. H. Chetwynd Jr., S. C. Richtmeier, B. Pukall, C. L. Allred, L. S. Jeong, and M. L. Hoke, "MODTRAN4 radiative transfer modeling for atmospheric correction," *Optical Spectroscopic Techniques and Instrumentation for Atmospheric and Space Research III. Proceedings of SPIE.*, vol. 3756 pp. 348-352, 1999.

Berk, A., L. S. Bemstein, and D. C. Robertson, "MODTRAN: A moderate resolution model for LOWTRAN 7," Burlington, MA, Spectral Sciences, Inc., Rep. GL-TR-89-0122, 1989.

Dozier, J. and S. G. Warren, "Effect of viewing angle on the infrared brightness temperature of snow," *Water Resour. Res.*, vol. 18, no. 5, pp. 1424-1434, 1982.

Gillespie, A. R., S. Rokugawa, T. Matsunaga, J. S. Cothern, S. Hook, and A. B. Kahle, "A temperature and emissivity separation algorithm for Advanced Spaceborne Thermal Emission and Reflection Radiometer (ASTER) images," *IEEE Trans. Geosci. Remote Sens.*, vol. 36, pp. 1113-1126, 1998.

Guenther, B., X. Xiong, V. V. Salomonson, W. L. Barnes, and J. Yong, "On-orbit performance of the Earth Observing System Moderate Resolution Imaging Spectroradiometer; first year of data," *Remote Sens. Environ.*, vol. 83, no. 1-2, pp. 16-30, 2002.

Irbe, G. J., *Great Lakes Surface Water Temperature Climatology*, Ottawa: Canadian Government Publishing Centre, 1992.

Jin, M., and R. E. Dickinson, "Interpolation of surface radiative temperature measured from polar orbiting satellites to a diurnal cycle part 1. without clouds," *J. Geophys. Res.*, vol. 104, pp. 2105-2116, 1999.

Kahle, A. B., D. P. Madura, and J. M. Soha, "Middle infrared multispectral aircraft scanner data: analysis for geological applications,," *Appl. Optics*, vol. 19, pp. 2279-2290, 1980.

Kealy, P. S. and A. R. Gabell, "Estimation of emissivity and temperature using alpha coefficients," in *Proc. 2nd TIMS Workshop*, pp. 11-15, Pasadena, CA: Jet Propul. Lab., JPL Publication 90-55, 1990.

Kerr, Y. H., J. P. Lagouarde, and J. Imbernon, "Accurate land surface temperature retrieval from AVHRR data with use of an improved split window algorithm," *Remote Sens. Environ.*, vol. 41, no. 2-3, pp. 197-209, 1992.

Kneizys, F. X., E. P. Shettle, L. W. Abreu, J. H. Chetwynd, G. P. Anderson, W. O. Gallery, J. E. A. Selby, and S. A. Clough, "Users Guide to LOWTRAN 7," Bedford, MA, Air Force Geophys. Lab., Rep. AFGL-TR-88-0177, 1988.

Labed, J. and M. P. Stoll, "Angular variation of land surface spectral emissivity in the thermal infrared: laboratory investigations on bare soils," *Int. J. Remote Sens.*, vol. 12, no. 11, pp. 2299-2310, 1991.

Li, Z.-L. and F. Becker, "Feasibility of land surface temperature and emissivity determination from AVHRR data," *Remote Sens. Environ.*, vol. 43, no. 1, pp. 67-85, 1993.

Li, Z.-L., F. Becker, M. P. Stoll, and Z. Wan, "Evaluation of six methods for extracting relative emissivity spectra from thermal infrared images," *Remote Sens. Environ.*, vol. 69, no. 3, pp. 197-214, 1999.

Ma, X., Z. Wan, C. C. Moeller, W. P. Menzel, L. E. Gumley, and Y. Zhang, "Retrieval of geophysical parameters from Moderate Resolution Imaging Spectroradiometer thermal

infrared data: evaluation of a two-step physical algorithm," *Appl. Optics*, vol. 39, no. 20, pp. 3537-3550, 2000.

Ma, X.-L., Z. Wan, C. C. Moeller, W. P. Menzel, and L. E. Gumley, "Simultaneous retrieval of atmospheric profiles and land-surface temperature/emissivity from Moderate Resolution Imaging Spectroradiometer thermal infrared data: extension of a two-step physical algorithm," *Appl. Optics*, vol. 41, no. 20, pp. 909-924, 2002.

Malm, J. and L. Jönsson, "Water surface temperature characteristics and thermal bar evolution during Spring in Lake Ladoga," *Remote Sens. Environ.*, vol. 48, pp. 332-338, 1994.

Malm, J. and S. Zilitinkevich, "Temperature distribution and current system in a convective mixed lake," *Boundary-Layer Meteorol.*, vol. 71, pp. 219-234, 1994.

Masuoka, M., A. Flag, R.E. Wolfe, and F. Patt, "Key characteristics of MODIS data products," *IEEE Trans. Geosci. Remote Sens.*, vol. 36, no. 4, pp. 1313-1323, 1998.

Nerry, F., J. Labed, and M. P. Stoll, "Spectral properties of land surfaces in the thermal infrared, 1, Laboratory measurements of absolute spectral emissivity signatures," *J .Geophys. Res.*, vol. 95, no. B5, pp. 7027-7044, 1990.

Ottle, C. and M. Stoll, "Effect of atmospheric absorption and surface emissivity on the determination of land temperature from infrared satellite data," *Int. J. Remote Sens.*, vol. 14, no. 10, pp. 2025-2037, 1993.

Petitcolin, F. and E. Vermote, "Land surface reflectance, emissivity and temperature from MODIS middle and thermal infrared data," *Remote Sens. Environ.*, vol. 83, no. 1-2, pp. 112-134, 2002.

Plokhenko, Y. and W. P. Menzel, "The effects of surface reflection on estimating the vertical temperature-humidity distribution from spectral infrared measurements," *J. Appl. Meteorol.*, vol. 39, pp. 3-14, 2000.

Prata, A. J., "Land surface temperatures derived from the advanced very high resolution radiometer and the along-track scanning radiometer 2. experimental results and validation of AVHRR algorithms," *J. Geophys. Res.*, vol. 99, no. D6, pp. 13025-13058, 1994.

Price, J. C., "Land surface temperature measurements from the split window channels of the NOAA-7 AVHRR," *J. Geophys. Res.*, vol. 79, pp. 5039-5044, 1984.

Realmuto, V. J., "Separating the effects of temperature and emissivity: emissivity spectrum normalization," in *Proc. 2nd TIMS Workshop*, pp. 26-30, Pasadena, CA: Jet Propul. Lab., JPL Publication 90-55, 1990.

Rees, W. G. and S. P. James, "Angular variation of the infrared emissivity of ice and water surfaces," *Int. J. Remote Sens.*, vol. 13, no. 15, pp. 2873-2886, 1992.

Salisbury, J. W. and D. M. D'Aria, "Emissivity of terrestrial materials in the 8-14 μm atmospheric window," *Remote Sens. Environ.*, vol. 42, no. 2, pp. 83-106, 1992a.

Salisbury, J. W. and D. M. D'Aria, "Infrared (8-14 μm) remote sensing of soil particle size," *Remote Sens. Environ.*, vol. 42, no. 2, pp. 157-165, 1992b.

Snyder, W. and Z. Wan, "BRDF models to predict spectral reflectance and emissivity in the thermal infrared," *IEEE Trans. Geosci. Remote Sens.*, vol. 36, no. 1, pp. 214-225, 1998.

Snyder, W. and Z. Wan, "Surface temperature correction for active infrared reflectance

measurements of natural materials," *Appl. Optics*, vol. 35, no. 13, pp. 2216-2220, 1996.

Snyder, W., Z. Wan, Y. Zhang, and Y.-Z. Feng, "Requirements for satellite land surface temperature validation using a silt playa," *Remote Sens. Environ.*, vol. 61, no. 2, pp. 279-289, 1997a.

Snyder, W., Z. Wan, Y. Zhang, and Y.-Z. Feng, "Thermal infrared (3-14 μm) bidirectional reflectance measurements of sands and soils," *Remote Sens. Environ.*, vol. 60, no. 1, pp. 101-109, 1997b.

Snyder, W. C., Z. Wan, Y. Zhang, and Y.-Z. Feng, "Classification-based emissivity for land surface temperature measurement from space," *Int. J. Remote Sens.*, vol. 19, no. 14, pp. 2753-2774, 1998.

Sobrino, J. A., C. Coll, and V. Caselles, "Atmospheric corrections for land surface temperature using AVHRR channel 4 and 5," *Remote Sens. Environ.*, vol. 38, no. 1, pp. 19-34, 1991.

Vidal, A., "Atmospheric and emissivity correction of land surface temperature measured from satellite using ground measurements or satellite data," *Int. J. Remote Sens.*, vol. 12, no. 12, pp. 2449-2460, 1991.

Wan, Z., "Estimate of noise and systematic error in early thermal infrared data of the Moderate Resolution Imaging Spectroradiometer (MODIS)," *Remote Sens. Environ.*, vol. 80, no. 1, pp. 47-54, 2002.

Wan, Z. and J. Dozier, "A generalized split-window algorithm for retrieving land-surface temperature from space," *IEEE Trans. Geosci. Remote Sens.*, vol. 34, no. 4, pp. 892-905, 1996.

Wan, Z. and J. Dozier, "Land-surface temperature measurement from space: physical principles and inverse modeling," *IEEE Trans. Geosci. Remote Sens.*, vol. 27, no. 3, pp. 268-278, 1989.

Wan, Z. and Z.-L. Li, "A physics-based algorithm for retrieving land-surface emissivity and temperature from EOS/MODIS data," *IEEE Trans. Geosci. Remote Sens.*, vol. 35, no. 4, pp. 980-996, 1997.

Wan, Z., Y. Zhang, X. Ma, M. D. King, J. S. Myers, and X. Li, "Vicarious calibration of the Moderate-Resolution Imaging Spectroradiometer Airborne Simulator thermal infrared channels," *Appl. Optics*, vol. 38, no. 20, pp. 6294-6306, 1999.

Wan, Z., Y. Zhang, Z.-L. Li, R. Wang, V. V. Salomonson, A. Yves, and R. Bosseno, "Preliminary estimate of calibration of the Moderate Resolution Imaging Spectroradiometer (MODIS) thermal infrared data using Lake Titicaca," *Remote Sens. Environ.*, vol. 80, no. 3, pp. 497-515, 2002a.

Wan, Z., Y. Zhang, Q. Zhang, and Z.-L. Li, "Validation of the land-surface temperature products retrieved from Terra Moderate Resolution Imaging Spectroradiometer data," *Remote Sens. Environ.*, vol. 83, no. 1-2, pp. 163-180, 2002b.

Wan, Z., P. Wang, and X. Li,, "Using MODIS land-surface temperature and normalized difference vegetation index products for monitoring drought in the Southern Great Plains, USA," *Int. J. Remote Sens.*, vol. 25, no. 1, pp. 61-72, 2004a.

Wan, Z., Y. Zhang, Q. Zhang, and Z.-L. Li, "Quality assessment and validation of the MODIS global land-surface temperature," *Int. J. Remote Sens.*, vol. 25, no. 1, pp. 261-274, 2004b.

Watson, K., "Spectral ratio method for measuring emissivity," *Remote Sens. Environ.*, vol. 42, no. 2, pp. 113-116, 1992.

Wiscombe, W. J., "Extension of the doubling method to inhomogeneous sources," *J. Quant. Spectrosc. Radiat. Transf.*, vol. 16, no. 6, pp. 477-486, 1976.

Wiscombe, W. J. and J. W. Evans, "Exponential-sum fitting of radiative transmission functions," *J. Comp. Phys.*, vol. 24, no. 4, pp. 416-444, 1977.

Wolfe, R. E., M. Nishihama, A. J. Fleig, J. A. Kuyper, D. P. Roy, J. C. Storey, and F. S. Patt, "Achieving sub-pixel geolocation accuracy in support of MODIS land science," *Remote Sens. Environ.*, vol. 83, no. 1-2, pp. 31-49, 2002.